

71-27,631

MEHDIZADEH, Parviz, 1938-

THE EFFECTS OF ANODIC OXIDE FILMS ON
THE MECHANICAL PROPERTIES OF ALUMINUM
SINGLE CRYSTALS.

The University of Oklahoma, Ph.D.,
1971
Materials Science

University Microfilms, A XEROX Company, Ann Arbor, Michigan

THE UNIVERSITY OF OKLAHOMA

GRADUATE COLLEGE

THE EFFECTS OF ANODIC OXIDE FILMS ON
THE MECHANICAL PROPERTIES OF ALUMINUM SINGLE CRYSTALS

A DISSERTATION

SUBMITTED TO THE GRADUATE FACULTY

in partial fulfillment of the requirements for the

DOCTOR OF PHILOSOPHY

BY

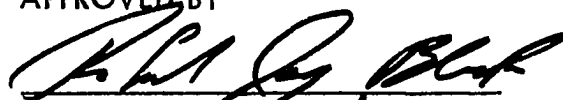
PARVIZ MEHDIZADEH

Norman, Oklahoma

1971

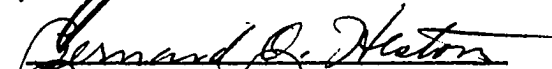
THE EFFECTS OF ANODIC OXIDE FILMS ON THE
MECHANICAL PROPERTIES OF ALUMINUM SINGLE CRYSTALS

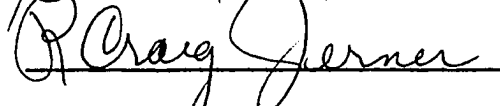
APPROVED BY











DISSERTATION COMMITTEE

ACKNOWLEDGEMENT

I sincerely wish to thank Dr. Robert J. Block for his help and guidance in all phases of this investigation.

I am greatly indebted to my wife, Dee, for her patience and understanding throughout the course of this work.

Sincere thanks and appreciation go also to Messrs. David Brown and Ronnie G. Smith for their assistance in the performance of various aspects of this work.

This investigation was sponsored by the U.S. Atomic Energy Commission.

ABSTRACT

The fracture strain of the anodic coatings formed on aluminum single and polycrystalline specimens was found to decrease as the thickness of the film was increased. Stress analysis applied to the coating crystal system indicated that the coatings were under the influence of a system of biaxial stresses. Thus, the magnitude of the coating fracture strains obtained in the present work was less than the fracture strain values reported for isolated anodic films of the same thickness.

Coatings thicker than 1350 \AA accommodated substrate strain by detachment at the slip steps and fracturing transverse to the tensile axis. The angle between the transverse cracks and the tensile axis of the single crystal specimen could be predicted from the specimen geometry and the orientation of the single crystal.

Coatings with thicknesses less than 900 \AA fractured at the slip steps, separating the film into strips. Transverse cracking then took place according to the state of the local substrate strains, which was in turn influenced by the positions of the surface relative to the slip vector. Whenever transverse cracking occurred, the crack density reached a plateau and further deformation merely opened the existing cracks. The equilibrium crack density was a function of the coating thickness. Consideration of this phenomenon indicated that elastic relaxation of the film subsequent to cracking inhibited the formation of new cracks. Further deformation of the film-substrate system induced preferential deformation of the substrate in the existing cracks.

Metallographic examination of the anodized single crystal specimens which were deformed until cracking and film buckling had taken place showed that "surface damage" in the form of suppression of surface slip and preferential deformation of the substrate in the cracks had occurred. Both thick and thin films induced surface damage where transverse cracking had occurred. Thick coatings had lower crack densities but preferential deformation at the cracks was extensive. Thin coatings, on the other hand, introduced a large number of cracks, but the extent of preferential deformation of the substrate in the cracks was less.

The effects of anodized coatings with compressive and tensile residual stresses on the stage I stress-strain parameters of the aluminum single crystals were determined. Based on the data available in the literature it was assumed that those anodic films formed at low formation rates were in compression, while the films formed at high formation rates had tensile residual stresses.

In general, the critical resolved shear stress increased when the single crystal specimens were anodized. For those anodic films formed at low rates, the extent of easy glide a_2 , the slope θ_1 and the stress at the start of stage II, τ_2 , increased relative to the uncoated crystals. The magnitudes of these changes were larger for thicker coatings. The stress-strain curves obtained from the specimens with the compressive anodic coatings crossed those of their control tests.

Coatings formed at high rates produced a decrease in the duration of stage I, a_2 , and an increase in θ_1 and τ_2 . Again, the effect was more pronounced for thicker coatings.

These effects can be explained in terms of the residual stresses in the coatings and the operation of the coating as a barrier to the egress of glide dislocations.

TABLE OF CONTENTS

	Page
LIST OF TABLES.....	iv
LIST OF ILLUSTRATIONS.....	v
INTRODUCTION.....	1
EXPERIMENTAL RESULTS AND DISCUSSION:.....	4
I. FRACTURE OF ANODIC FILMS.....	9
II. SURFACE DAMAGE.....	26
III. THE EFFECTS OF ANODIC FILMS ON THE PLASTIC DEFORMATION OF ALUMINUM SINGLE CRYSTALS (STAGE I).....	35
LIST OF REFERENCES.....	55
APPENDICES	
A. STRESS ANALYSIS OF COATING-SINGLE CRYSTAL COMPOSITE.....	58
B. COMPUTER PROGRAM TO OBTAIN SHEAR STRESS-SHEAR STRAIN PLOTS FROM LOAD-EXTENSION DATA.....	63
C. COMPUTER PROGRAM TO OBTAIN Θ_1 AND Θ_{11} FROM SHEAR STRESS-SHEAR STRAIN DATA.....	64

LIST OF TABLES

Table	Page
I. ORIENTATION OF CRYSTALS.....	5
II. CRACK ANGLES AND PRINCIPAL STRESS FUNCTIONS FOR ANODIC COATINGS ON CRYSTALS OF SQUARE CROSS SECTION.....	12
III. STRESS-STRAIN PARAMETERS OF THE SPECIMENS (STAGE I).....	38
IV. STRESS-STRAIN PARAMETERS OF THE SPECIMENS (STAGE II).....	39
V. CHANGES IN THE STAGE I STRESS-STRAIN PARAMETERS OF ALUMINUM SINGLE CRYSTALS DUE TO ANODIC FILMS.....	40
AI. VALUES OF DIFFERENT ANGLES USED IN THE CALCULATION OF THE PRINCIPAL STRAINS AND THE CRACK ANGLES.....	61
AII. VALUES OF THE STRAIN COMPONENTS USED IN THE CALCULATION OF THE PRINCIPAL STRAINS.....	61

LIST OF ILLUSTRATIONS

Figure		Page
1.	STEREOGRAPHIC REPRESENTATION OF THE ROUND (R) AND SQUARE (S-4A, B) CRYSTALS.....	6
2.	SCHEMATIC OF THE TEST CELL AND THE SPECIMEN GRIPPING SYSTEM.....	8
3.	FRACTURE STRAIN V.S. THE COATING THICKNESS.....	10
4.	TRANSVERSE CRACKS ON THE FACE A OF SPECIMENS S-4A, COATED WITH 3000 Å THICK ANODIC FILMS.....	11
5.	WIDENING OF THE TRANSVERSE CRACKS, SPECIMEN S-4A, 3000 Å THICK ANODIC FILM.....	14
6.	BUCKLING OF 1350 Å AND 3000 Å THICK ANODIZED COATINGS AFTER 14% AND 4% SUBSTRATE STRAIN.....	15
7.	BUCKLING OF 450 Å AND 750 Å THICK ANODIZED COATINGS AFTER 11% AND 7% SUBSTRATE STRAIN.....	16
8.	APPEARANCE OF 300 Å THICK COATING AFTER 18.5% SUBSTRATE ELONGATION.....	17
9.	INITIATION OF CRACKS AT THE DEFECTS.....	19
10.	SCHEMATIC DIAGRAM OF WAYS IN WHICH A FILM MAY ACCOMMODATE SLIP IN THE SUBSTRATE.....	21
11.	APPEARANCE OF THE SLIP STEPS AT THE SCREW (A) AND EDGE (B) POSITIONS OF SPECIMEN R-7-5, COATED WITH 300 Å THICK ANODIC FILMS, AFTER 4% SUBSTRATE ELONGATION.....	24
12.	DENSITY OF TRANSVERSE CRACKS V.S. SUBSTRATE STRAIN FOR ANODIC FILMS OF DIFFERENT THICKNESSES.....	27
13.	APPEARANCE OF THE SURFACE OF A SQUARE CRYSTAL COATED WITH 450 Å THICK ANODIC FILM; STRAINED 7.5%, BEFORE AND AFTER THE COATING WAS STRIPPED OFF.....	28
14.	APPEARANCE OF THE SURFACE OF SPECIMEN S-4A, COATED WITH 3000 Å THICK ANODIC COATING AND STRAINED 10%, BEFORE AND AFTER THE COATING WAS STRIPPED OFF.....	29

Figure		Page
15.	APPEARANCE OF THE SURFACE OF THE SPECIMEN S-4A, COATED WITH 3000 Å THICK ANODIC FILM AND STRAINED 10%, AFTER THE COATING WAS STRIPPED OFF AND UPON 3% FURTHER DEFORMATION.....	31
16.	STRESS DISTRIBUTION IN THE COATING, BETWEEN TWO INTER-ACTING TRANSVERSE CRACKS.....	32
17.	CONVENTIONS USED IN DETERMINING THE STRESS-STRAIN PARAMETERS OF ALUMINUM SINGLE CRYSTALS.....	37
18.	STRESS-STRAIN CURVES FOR COATED AND UNCOATED ALUMINUM SINGLE CRYSTALS INDICATING THE EFFECT OF 300 Å THICK ANODIC FILM WITH COMPRESSIVE RESIDUAL STRESSES....	41
19.	STRESS-STRAIN CURVES FOR COATED AND UNCOATED ALUMINUM SINGLE CRYSTALS INDICATING THE EFFECT OF 450 Å THICK ANODIC FILM WITH COMPRESSIVE RESIDUAL STRESS.....	42
20.	STRESS-STRAIN CURVES FOR COATED AND UNCOATED ALUMINUM SINGLE CRYSTALS, INDICATING THE EFFECT OF 1350 Å THICK ANODIC FILM WITH COMPRESSIVE RESIDUAL STRESS.....	43
21.	STRESS-STRAIN CURVES FOR COATED AND UNCOATED ALUMINUM SINGLE CRYSTALS INDICATING THE EFFECT OF 3000 Å THICK ANODIC FILM WITH COMPRESSIVE RESIDUAL STRESS.....	44
22.	STRESS-STRAIN CURVES FOR COATED AND UNCOATED ALUMINUM SINGLE CRYSTALS INDICATING THE EFFECT OF 1350 Å THICK ANODIC FILM WITH TENSILE RESIDUAL STRESS.....	45
23.	STRESS-STRAIN CURVES FOR COATED AND UNCOATED SINGLE CRYSTALS INDICATING THE EFFECT OF 450 Å AND 3000 Å THICK ANODIC FILMS WITH TENSILE RESIDUAL STRESS.....	46
24.	LOAD-POTENTIAL-EXTENSION CURVES FOR SPECIMEN R-15-1, COATED WITH 3000 Å THICK ANODIC FILM.....	50
25.	LOAD-POTENTIAL-EXTENSION CURVES FOR SPECIMEN R-7-5, COATED WITH 300 Å THICK ANODIC FILM.....	51

Figure		Page
1A.	GEOMETRIC CONVENTIONS USED IN THE CALCULATION OF THE STRAIN COMPONENTS AND THE CRACK ANGLES.....	59

INTRODUCTION

It is now well established that the condition of the surface can strongly influence the plastic deformation of metals. These effects have been adequately reviewed elsewhere (1,2,3). Numerous experimental studies of a variety of systems have been conducted to arrive at the mechanism through which surface conditions affect the mechanical properties of materials. A particular area that has received considerable attention in recent years is the effect on the mechanical properties of metals of the presence of thin metallic films and oxide coatings on their surface.

In the present work, we direct our attention to the behavior of anodic oxide films on aluminum single crystals and their effects on the mechanical properties. A brief review of the previous work appropriate to this aspect of the problem will be presented.

In 1934, the pioneering work by Roscoe (3) showed that thin films of oxide, less than twenty atoms thick, increased the strength of cadmium single crystals. A number of other investigations have confirmed the strengthening effect of oxide films. The mechanical behavior has been studied using (1) tensile deformation (2,4,5,6), torsion (7,8), creep (4), and fatigue (10).

As a result of torsion experiments, Barrett (8) reported that an aluminum wire with an adherent oxide coating on the surface deformed by positive torsion experienced a further increment of positive torsion when the coating was removed. This abnormal after-effect was much greater with thick porous, sulphuric acid type anodic films than with the thin dense type produced in boric acid, or with films formed in air or water. Edelson and Robertson (11) reported that the abnormal after-effect increases with increasing anodic film thickness.

Two principal models have been proposed to explain these observations. Barrett (8), following a suggestion by Cottrell, proposed the now classic dislocation model, according to which the effect was attributed to the release of dislocation pile-up upon removal

of the oxide. Edelson and Robertson (11) accounted for the Barrett after-effect on the basis of a simple two-component mechanical system. In their model the normal recovery of the twisted wire is altered by the elastic stresses imposed by coatings of higher modulus of elasticity. Thus, upon removing the film, the wire reverts to a strain and strain rate it would have had in the absence of the coating. This requires a reversal of the untwisting process which is the abnormality in the after-effect.

Jemain and Law (12) investigated the effects of various metallic coatings on torsional after-effect using copper and gold wires. Their results show that a distinct abnormal after-effect is observed regardless of the relative magnitude of the moduli of the substrate and coating. These results also demonstrate that the abnormal after-effect is better explained in terms of dislocation release models rather than the two-component mechanical system.

Experiments to measure the effect of oxide coatings on the torsion and tensile behavior of aluminum crystals were performed by Takamura (5). It was found that the amount of crystal rotation during plastic deformation was a very sensitive measure of slip. Thick oxide coatings (500 \AA) increased the flow stress and suppressed crystal twisting during the extension. These effects were thought to be due to dislocation pile up beneath the surface film. Takamura also noted that the entire stress-strain curves were usually raised due to the presence of surface films.

The suppression of surface slip by anodic films on aluminum has also been noted by Alden and Backofen (10) and Grosskreutz (13) and is attributed to the surface-film blocking of dislocations approaching the surface.

Johnson and Block (14) tried to distinguish among the film strengthening mechanisms using copper single crystals with a variety of coatings. These mechanisms may be grouped into three broad categories: (A) the coating acts as a barrier to the egress of dislocations (2, 7, 10), (B) elastic repulsion of dislocations in the substrate by a coating of higher modulus

(15,16), and (C) the pinning of surface Frank-Read sources by the coating (17,18,19). Johnson and Block found that none of the above mechanisms played the dominant role in the systems they studied. Significant film strengthening was always accompanied by film cracking either prior to or during deformation as a result of residual stresses in the coating. Associated with film cracking was an increase in dislocation density in the substrate. This "surface damage" was believed to be the critical factor in producing the film strengthening effects they observed.

The present investigation was aimed at resolving the relationship between the behavior of anodic oxide films during deformation and their effect on the stress-strain parameters of the aluminum single crystals. The results will be treated in three sections: Part I considers the fracture of anodic oxide films; Part II, the role played by "surface damage"; and Part III, the relationship between the fracture characteristics of the anodic films and the changes in the stress-strain parameters of the aluminum single-crystal substrate.

EXPERIMENTAL

Single crystals of 99.99+ % aluminum were grown in spectroscopically pure graphite molds using a modified Bridgman technique. Crystals of round cross section 1/8 inch in diameter and square cross section 1/8 inch on a side were produced. The round crystals were orientated for maximum easy glide. The orientations were determined by the Laue back reflection technique and are presented in Table I and Figure 1.

The as-grown crystals were cut into 1 3/4" long tensile specimens and annealed at 618°C for 24 hours. Tensile specimens of 1-inch gauge length were prepared by gluing 5/16-inch diameter glass balls on each end of the cut crystals using Armstrong A-1 epoxy adhesive. The mounting procedure results in electrical insulation of the specimen. A flexible lead was attached to one end of the specimen to allow electrical contact with the specimen during the electropolishing and anodizing operations. The specimens were electropolished at 200 ma/cm² in a 5:1 ethanol: perchloric acid electrolyte held at 20°F. This was followed by oxide stripping in a solution consisting of orthophosphoric acid (20%), chromium trioxide (20%), and water held at 90°C.

Anodic coatings were formed in 0.4 M boric acid solution, buffered to a pH of 5.5 with ammonium hydroxide, immediately after the stripping and rinsing operations. The current density during anodizing was maintained below the required limit by increasing voltage in steps, and allowing the current to drop to a steady leakage value. The oxide thickness was determined from the voltage assuming 14 Å per volt. (20)

Mechanical testing was carried out on an Instron machine at the strain rate of $2 \times 10^{-2} \text{ min}^{-1}$. The balls at each end of the specimen fitted into specially machined grips of the testing machine. Axiality was achieved through the use of a positive alignment jig, which also permitted removal and re-insertion of the specimen without the loss of alignment.

TABLE I
ORIENTATION OF CRYSTALS

Specimen Designation	λ_o	ϕ_o
R*-6	49°	42.5°
R-7	50.5°	42°
R-10	45°	47°
R-11	51.5°	42°
R-15	44°	47°
R-16	46°	46°
R-17	48°	48°
S**-4A	47°	42°
S-4B	37°	53°

R* Round Cross Section

S** Square Cross Section

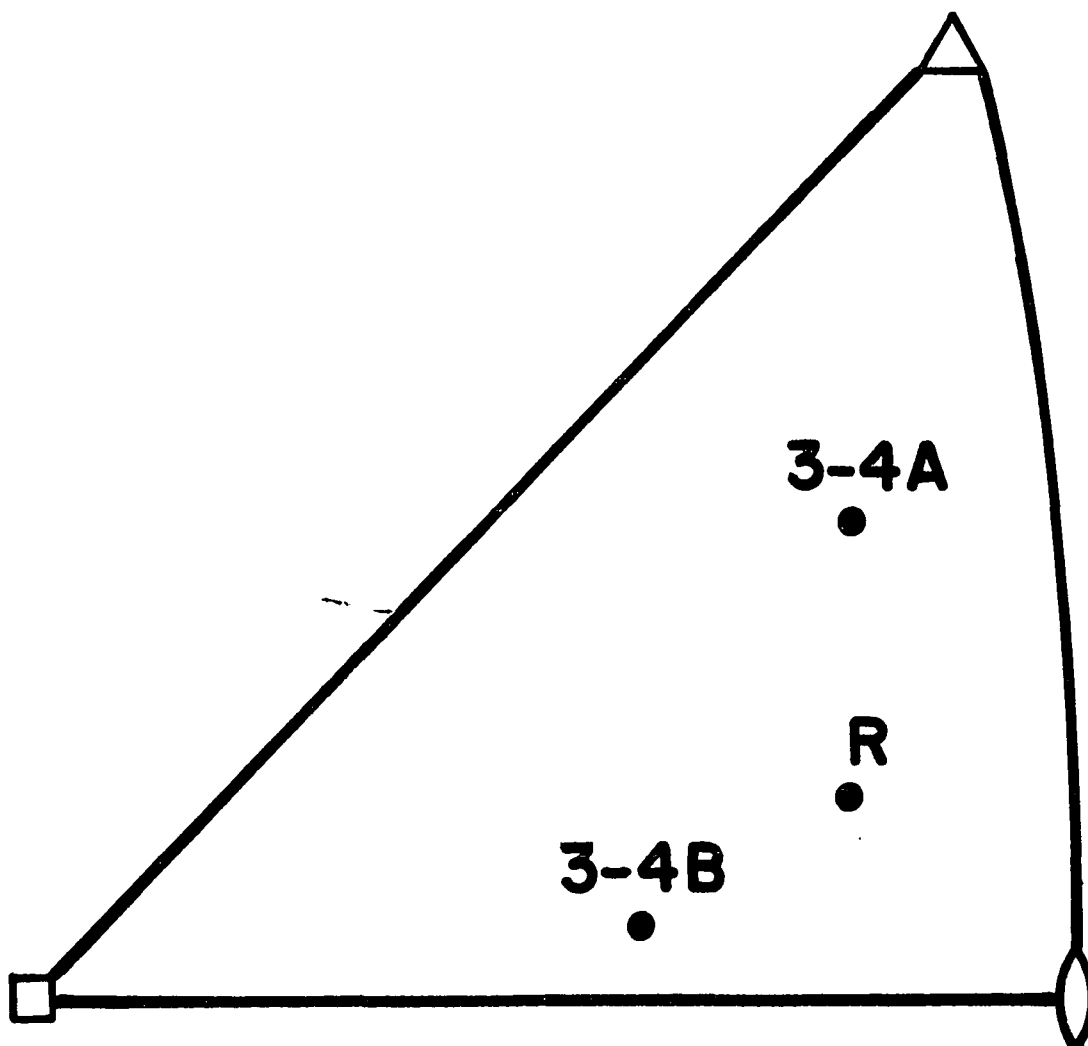


FIG. 1 - Stereographic representation of round (R) and square (3-4A,B) crystals used.

Method of Detecting Film Failure

The potential method was used to detect the film failure during tensile tests. A diagram of the test cell and the specimen gripping system is shown in Figure 2. The open circuit potential of the anodized aluminum specimen was 300-500 mv anodic relative to the reference calomel electrode. When the underlying metal was exposed to the electrolyte, due to the fracture of the oxide coating, the potential changed. Potential changes were measured by using a high impedance voltmeter. A two-pen recorder was used to plot potential and load vs. elongation.

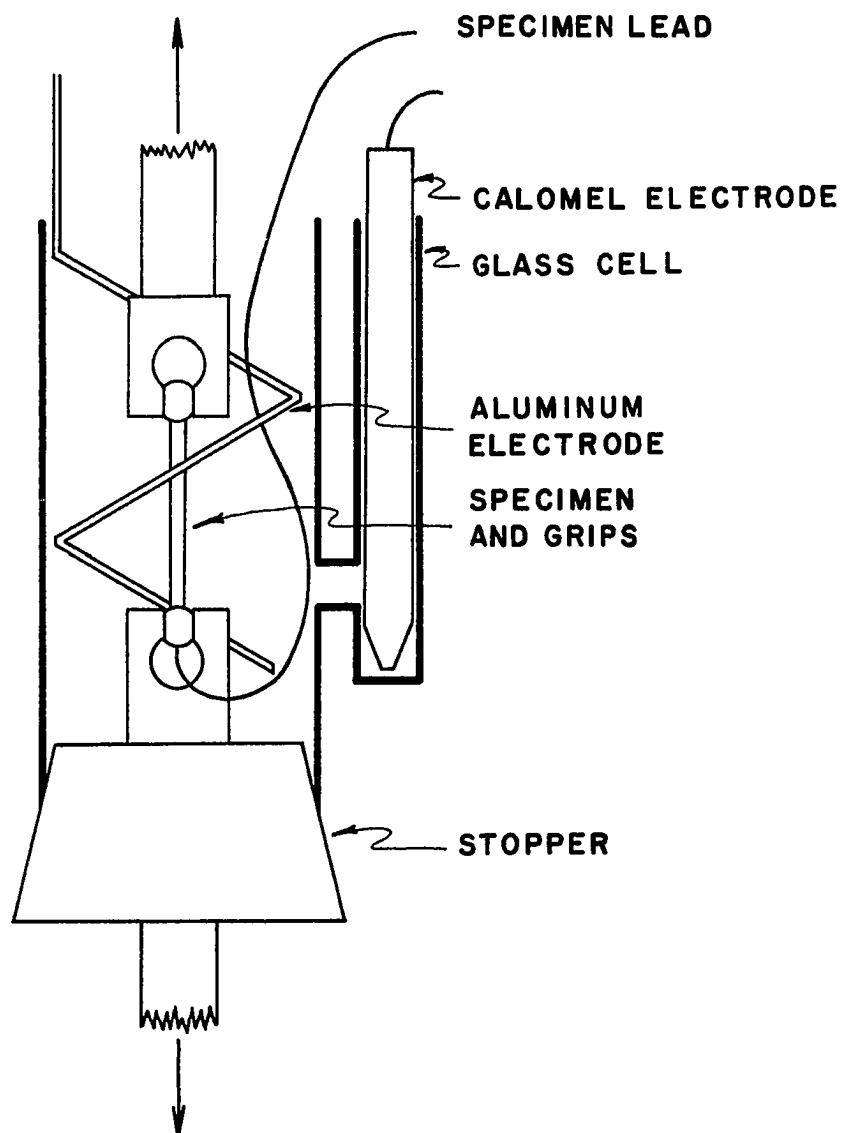


FIG. 2 - Schematic of the test cell and the specimen gripping system.

I - FRACTURE OF THE ANODIC FILMS

Results:

The fracture strains of anodized coatings of various thicknesses are shown in Figure 3. The data were obtained from round single crystals of similar orientation as noted in Table I. The fracture strain was found to decrease as the coating thickness was increased. Metallographic study of the coated and deformed specimens revealed a distinct difference in the mode of deformation of the coatings as the coating thickness was increased. The mechanisms by which the coating accommodated the substrate strain will be discussed in the following sections.

Behavior of Thick Coatings:

Coatings thicker than 1350 \AA always failed by transverse cracking. Metallographic examination of a large number of specimens showed (as in Figure 4) that the direction of cracking was not necessarily perpendicular to the tensile axis as reported elsewhere (21). Stress analysis applied to the coating-single crystal composite (Appendix A) indicated that thick coatings always cracked transverse to the direction of principal stress. Table II shows the observed and calculated crack angles along with the principal stress in the coating as a function of substrate shear strain for different faces of the specimens S-4A and S-4B (See Appendix A). It should be noted that the coating reacts to a system of biaxial stresses.

Metallographic observation of thick coatings on specimens of square cross section, just after the first cracks were detected by the potential method, showed that the thick coatings always cracked preferentially on one face. This preferential cracking could be predicted from the orientation dependence of the principal stress in the coating as shown in Table II.

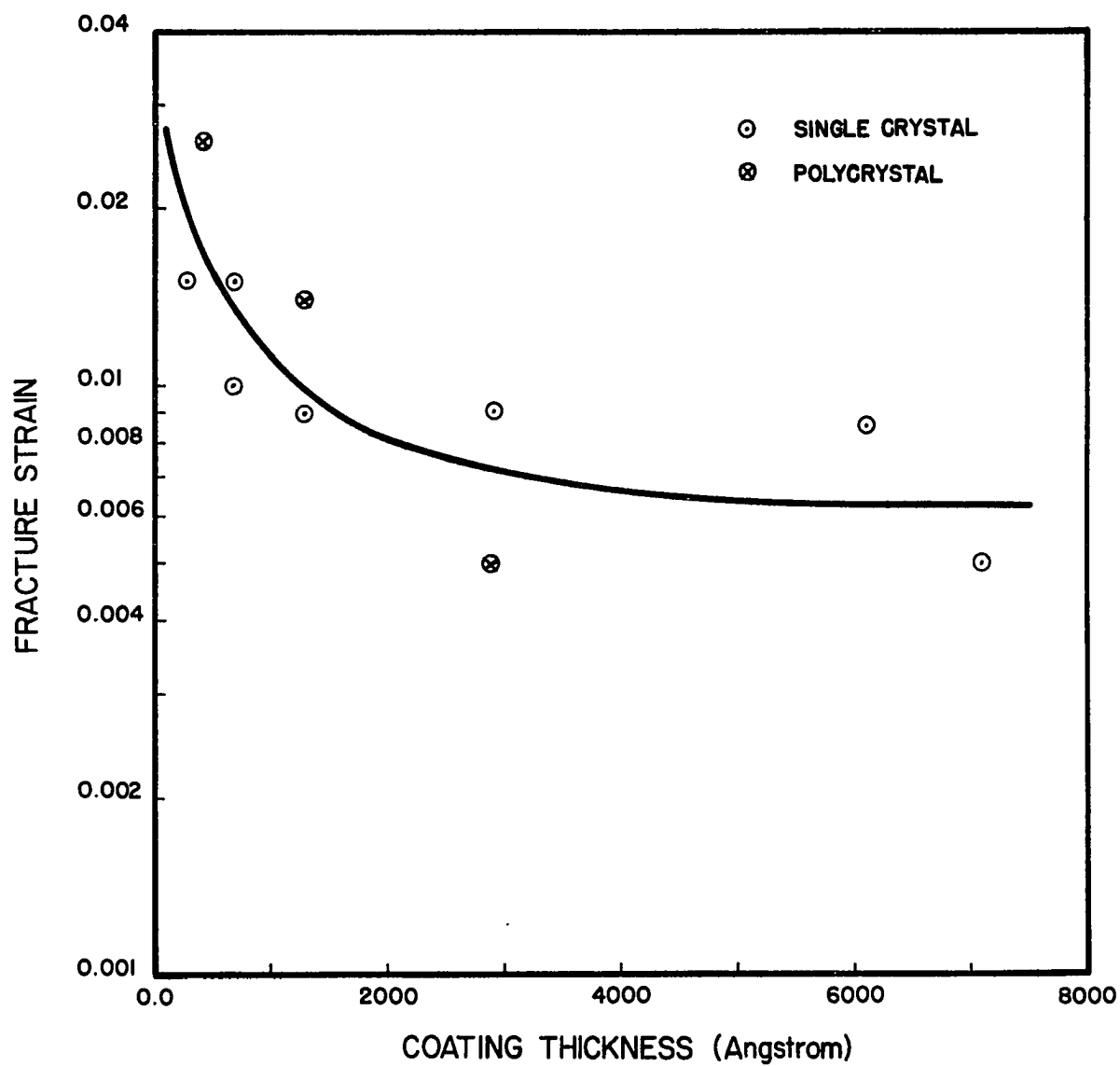


FIG. 3 - The fracture strain v.s. the coating thickness.

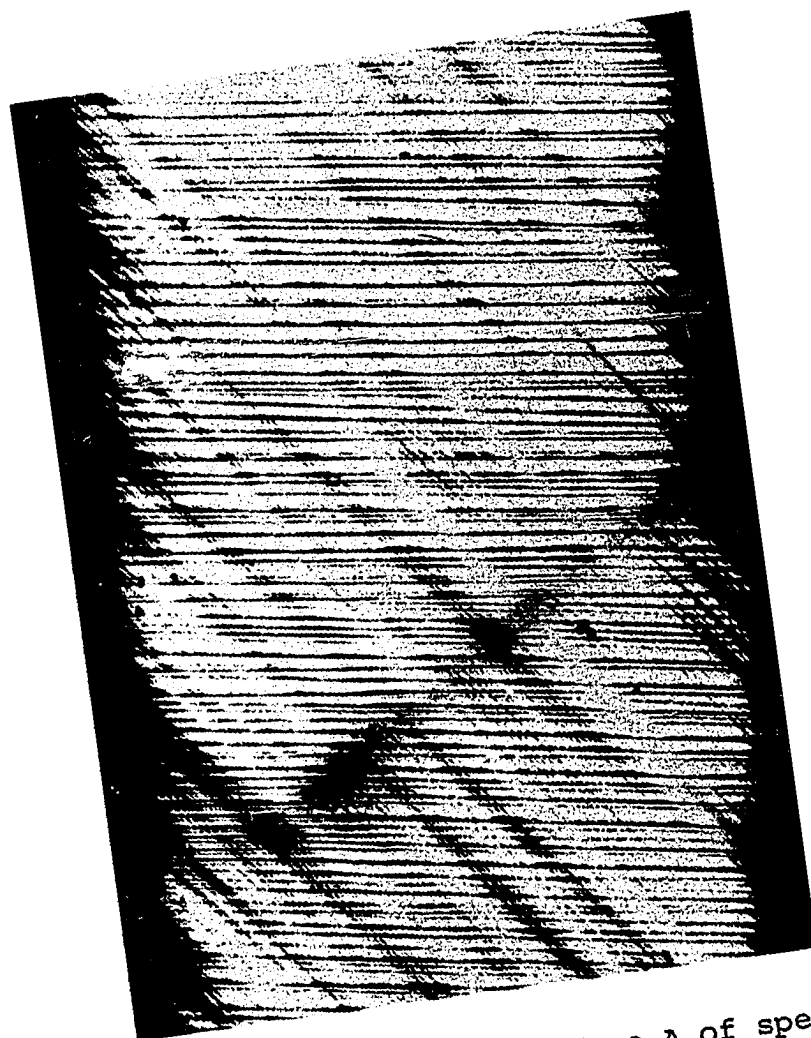


FIG. 4 - Transverse cracks on the face A of specimen S-4A, coated with 3000 Å thick anodic film. The angle between the cracks and the tensile axis of the specimen is 79°. 50X

TABLE II
CRACK ANGLES AND PRINCIPAL STRESS FUNCTIONS FOR ANODIC COATINGS
ON CRYSTALS OF SQUARE CROSS SECTION

SPECIMEN	ANGLE (T.A. - CRACK) \ominus				σ_1^c = PRINCIPAL STRESS FUNCTION	
DESIGNATION	OBSERVED		CALCULATED		FACE A	FACE B
	FACE A	FACE B	FACE A	FACE B		
S-4A	79	94	75	94	$\sigma_1^c = 0.631 E_c \gamma$	$\sigma_1^c = 0.726 E_c \gamma$
S-4B	92	77	92	73	$\sigma_1^c = 0.839 E_c \gamma$	$\sigma_1^c = 0.705 E_c \gamma$

The crack density increased with the strain up to a limiting value. Thereafter further strain was accommodated by crack widening and new cracks did not form. This is illustrated in Figure 5 with a specimen (S-4A) having a 3000 \AA coating. The dark diagonal markings seen in the cracks of Figure 5 are slip steps. It may be seen in Figure 5b that the cracks opened up considerably with continued strain and the slip steps became more pronounced. The vertical structures in Figure 5b are due to the buckling of the anodized film as the result of circumferential compressive strain (Table AII) on the specimen surface (22).

Buckling always initiated at the intersection of the slip steps and the transverse cracks. The width of the buckle was a function of the coating thickness and did not change with the strain. Figures 6 and 7 show buckling in coatings of other thicknesses.

Behavior of Thin Coatings

Cracking of the anodized coatings of thicknesses less than 900 \AA was influenced by the mode of deformation of the substrate. Figure 8 shows the appearance of a 300 \AA anodic coating (specimen R-7-5) after 18.5% elongation. Although this is considerably beyond the range of easy glide, slip line observations indicated that the surface layers of aluminum crystals exhibited coarse single slip into stage II and beyond. The sketch in this figure indicates the approximate location of the photomicrographs relative to the primary slip direction, as determined by the Laue method. As shown, the film fractured at the slip steps at positions near the slip vector (Figure 8d). For other positions, the transverse cracking mode was more dominant (Figures 8b,c). At position E, the fracture was mainly due to the transverse cracking, while at position A, transverse cracking did not develop.

The vertical markings in Figure 8a are buckles formed according to the mechanism proposed by Edeleanu and Law (23). The shape of these folds did not change but their density increased when the specimen was further deformed.

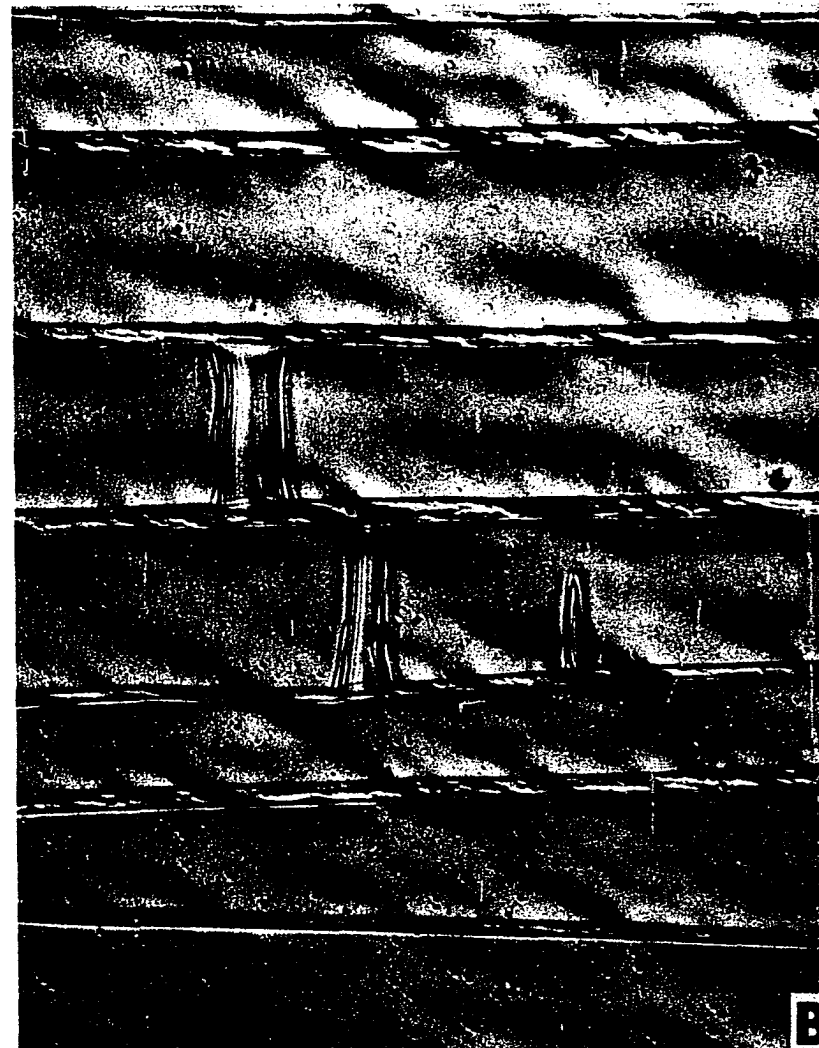


FIG. 5 - Widening of the transverse cracks, specimen S-4A, 3000 Å thick anodic film. (A) - 5.6% elongation. (B) - 10.5% elongation.

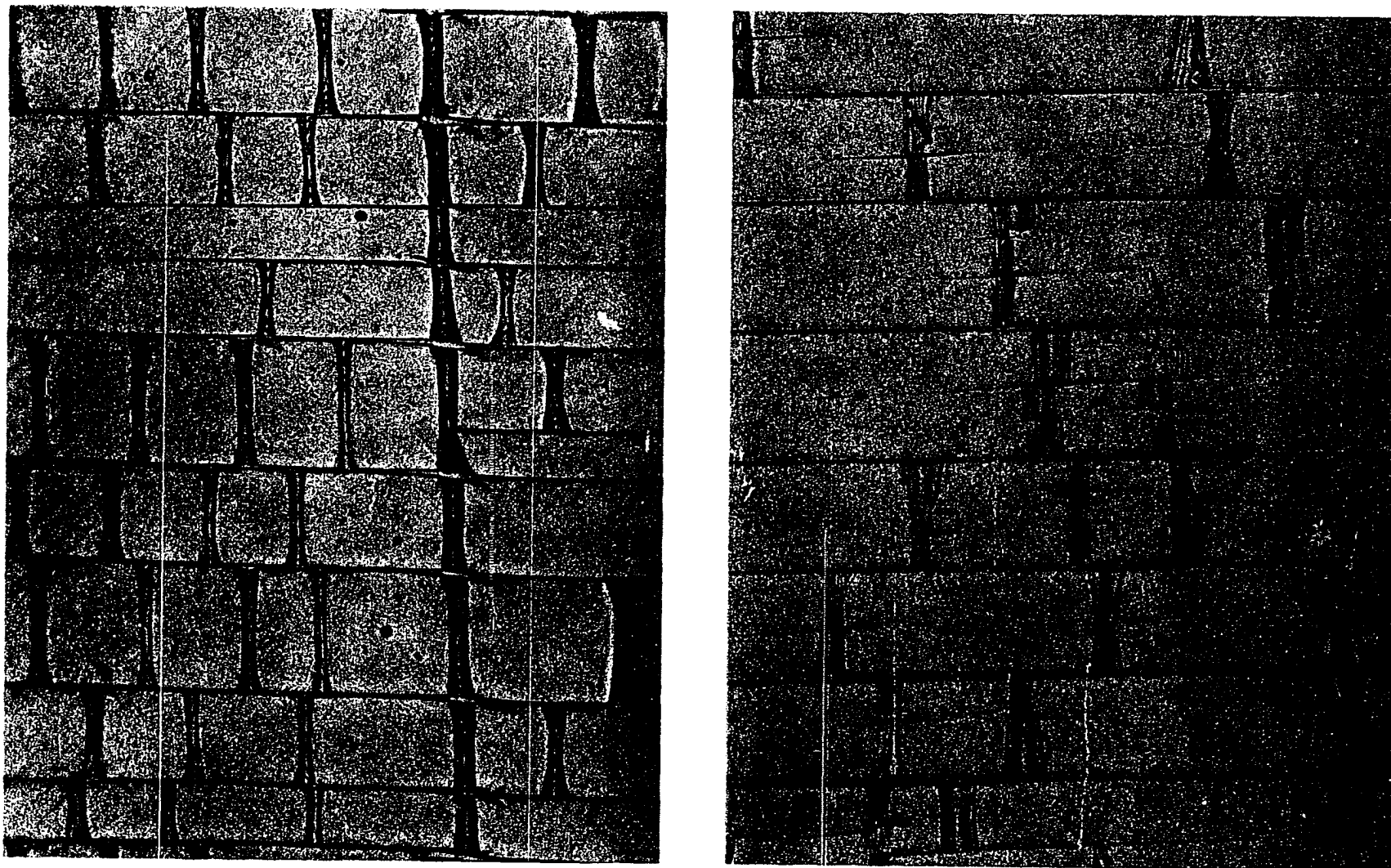


FIG. 6 - Buckling of 1350 Å thick (A) and 3000 Å thick (B) anodized coating after 14% and 4% substrate strain. 500X

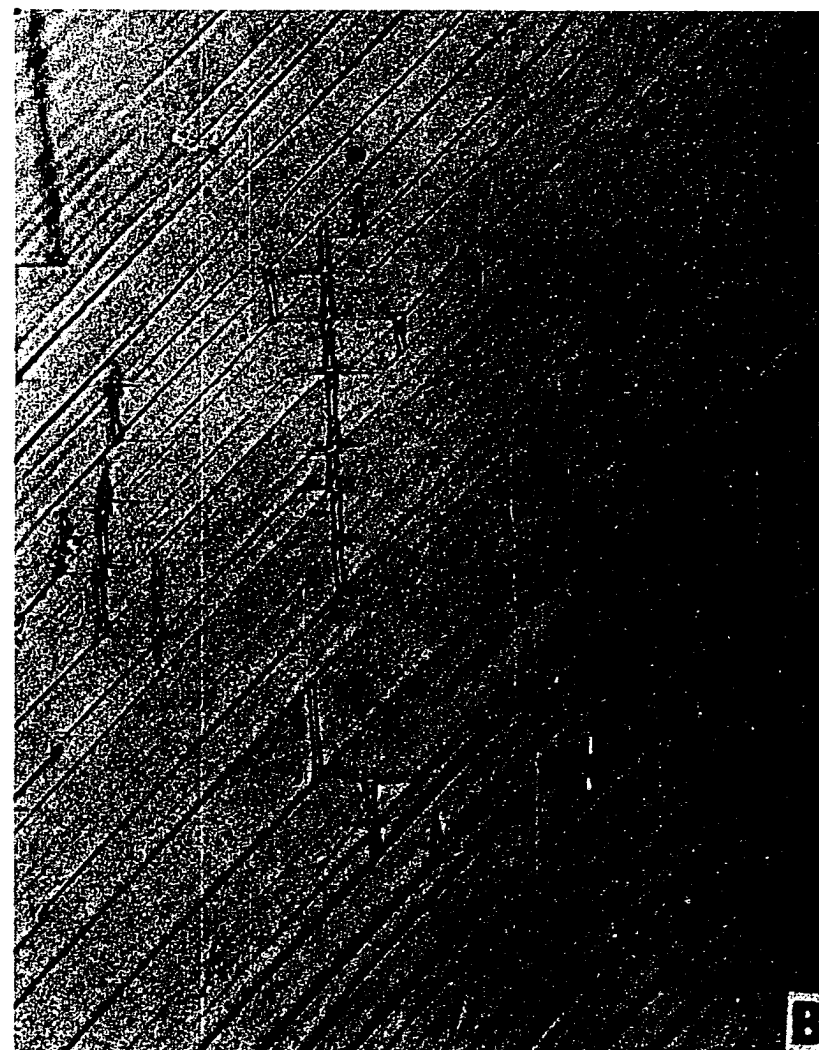
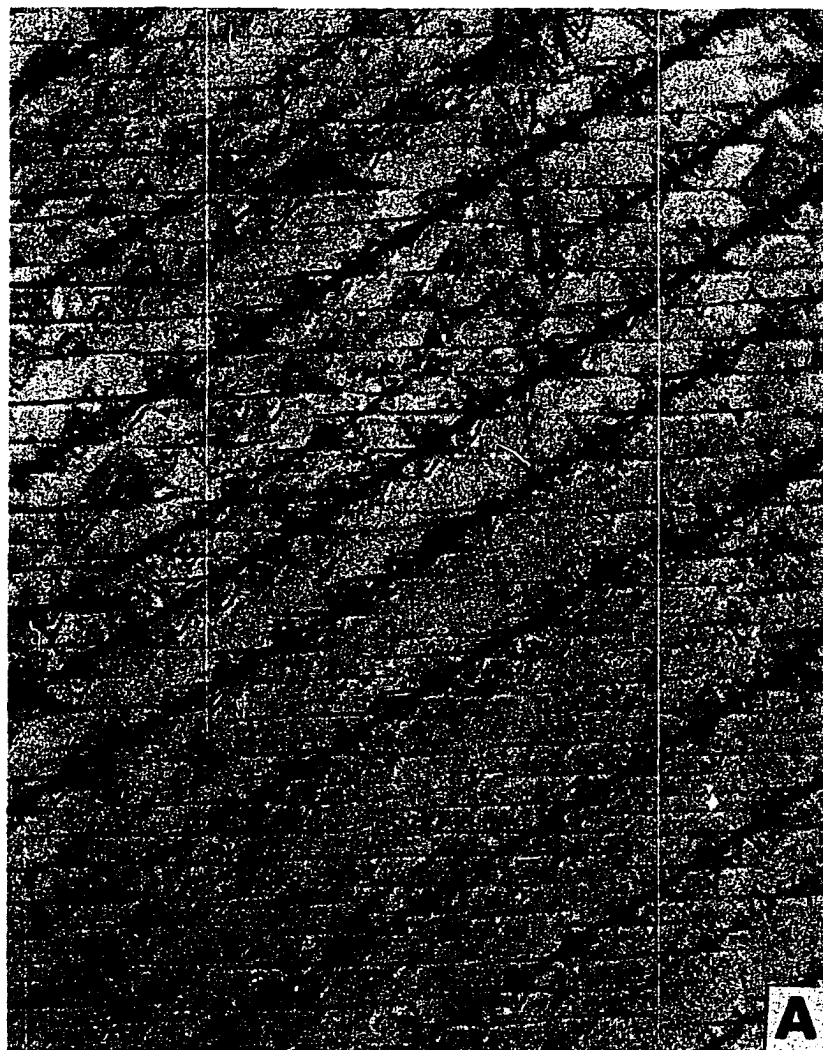


FIG. 7 - Buckling of 450 Å thick (A) and 750 Å thick (B) anodized coatings after 11% and 7% substrate strain. 500X

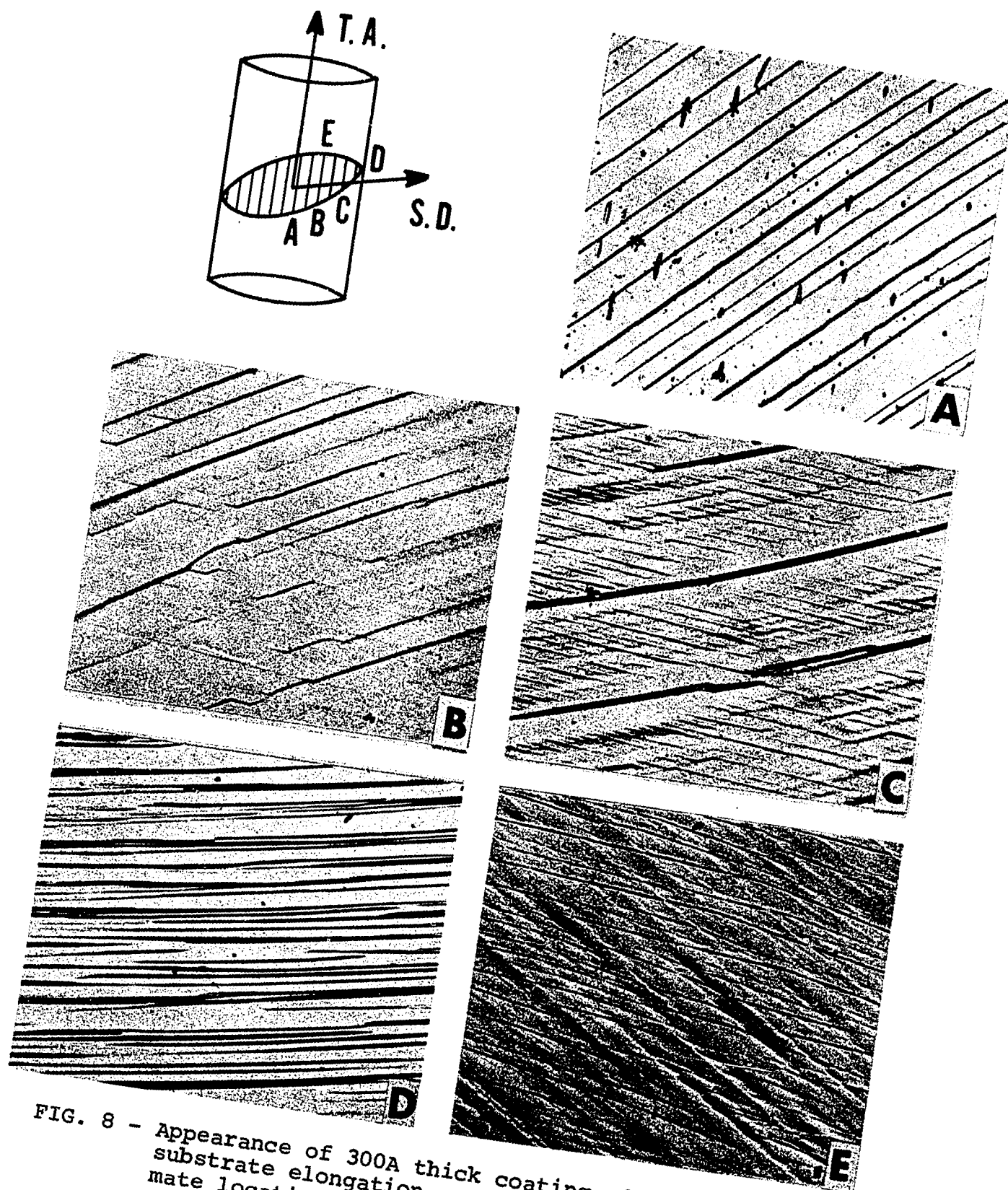


FIG. 8 - Appearance of 300A thick coating after 18.5% substrate elongation. The sketch shows approximate location of the micrographs relative to the slip direction of specimen R-7-5.

Discussion:

The features of anodic coatings which appear to influence the mechanical properties of the substrate may now be discussed. Initially, one has to explain the change in mechanical properties of the anodized films with increasing thickness (Figure 3). Bradhurst and Leach (24) have shown that the fracture strain of anodic films formed on thin (0.022") aluminum sheets decreased as the thickness of the film was increased. The behavior in the present work can not be due to changes in the mode of substrate deformation, since Figure 3 shows the same trend as that obtained from films on fine grain polycrystalline aluminum (24). Indeed, in the work cited above, the sheets were probably used in the as-deformed condition. Thick films were also difficult to produce with a high degree of perfection. Figure 9 shows a type of defect commonly found. These defects result from the formation of unwanted corrosion products such as hydroxides and represent regions of lower film strength and adherence. It may be seen in the figure that film cracking initiated in such defects and then propagated into the adjoining coating.

Another important factor which influences the fracture strain is the magnitude and nature of residual stresses produced during the growth of anodic films. Bradhurst and Leach (25) found that the residual stresses in the oxide, measured according to the method of Brenner and Senderoff (26), appeared to vary from 1000 kg/cm^2 for thin (400 \AA) coatings to 300 kg/cm^2 for thick ($3000 - 5000 \text{ \AA}$) coatings. It appears that the current density used for coating formation is the most influential factor in determining the nature of the stresses developed. Vermilyea (27) has reported that high rates of oxide formation tend to make the residual stresses more tensile in character. His results showed that residual stresses in a 2250 \AA film formed in ammonium borate solution doubled when the formation rate was changed from 2 ma/cm^2 to 20 ma/cm^2 (27). On the basis of their data on the residual stresses and those of Davis (28) on ionic transport during formation of the coatings. Bradhurst and Leach (25) suggested that anodic films formed below 1 ma/cm^2 should have low tensile or compressive residual stress, while films formed at higher rates will be in tension.

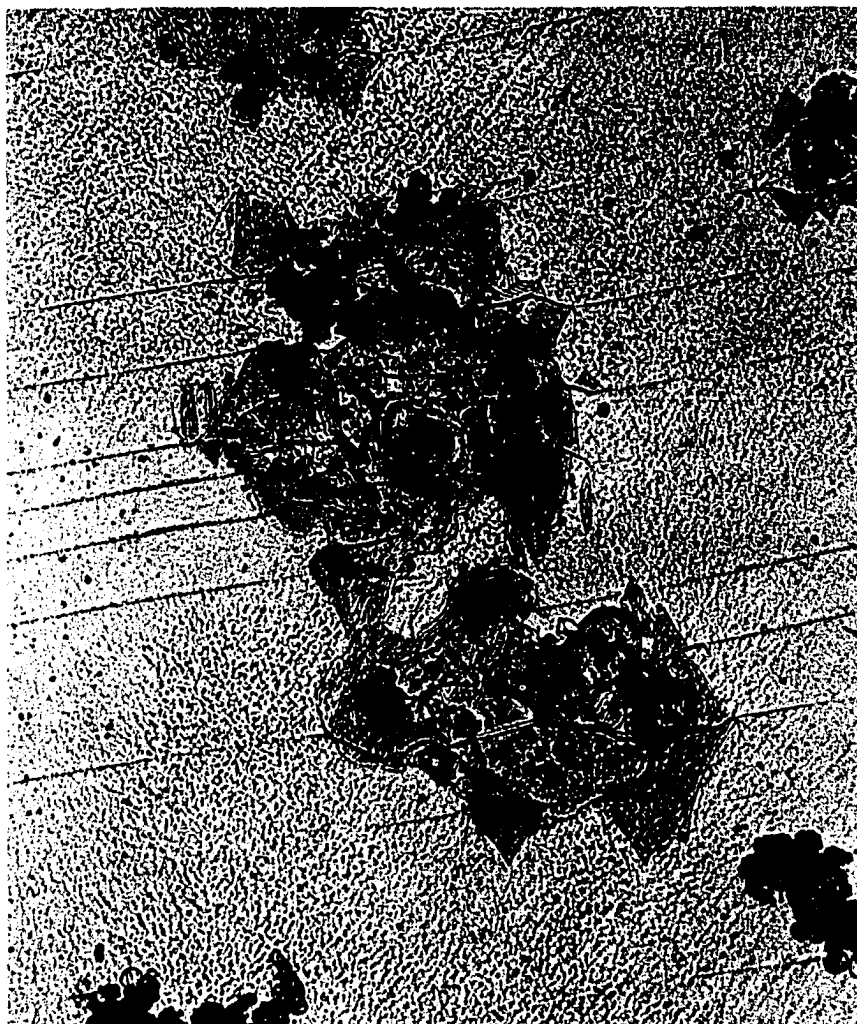


FIG. 9 - Note the initiation of cracks at the defects.
Square crystal with 1350 Å anodic film, after 2.3%
substrate deformation. 200X

In order to determine the effect of residual stresses on the fracture strain of the anodic films, the following experiment was performed. Two round aluminum single crystals of similar orientation were anodized to 200 volts using current densities ranging between $0.3 - 0.5 \text{ ma/cm}^2$ and $4 - 5 \text{ ma/cm}^2$, respectively. The fracture strain, as determined by the potential method, was 0.009 and 0.0035 respectively, suggesting that the residual stresses may be high enough to affect the fracture strain of the anodic films in-situ. It should be noted that coatings formed at high rates are not as smooth and clean as those formed at the low rates. They tended to show the type of defects previously discussed.

The results plotted in Figure 3 were obtained from films formed at 0.2 ma/cm^2 ; thus residual stress should not be an important factor. One might be tempted to attribute the observed behavior to changes in the structure of the coating as it thickens, since little is known about the details of its structure.

The mode of the fracture of surface coatings on strained substrates has been investigated by other workers. Brame and Evans (29) and Evans and Schwartzberger (30) investigated the fracture of metallic films on silver single crystals. More recently Grosskreutz and McNeil (31) examined the fracture of oxide films on metal substrates. The mode of fracture of any coating is determined by two factors: (1) mechanical properties of the coating, and (2) its adherence to the substrate. Figure 10 suggests the ways in which a coating may accommodate a slip step in the substrate. Cracking at slip steps can take place either by fracture or shear of an adherent coating (Figure 10a and 10c). On the other hand, if the film strength is sufficiently large or the adherence is low, the film detaches at the slip steps (Figure 10b).

Grosskreutz and McNeil (31) developed the following relations to describe the separation of a coating at the slip step (Figure 10c):

$$\lambda = E_c \left\{ \left[\epsilon / \sqrt{2} (1 + \nu) \right]^{1/2} (t/\alpha)^{1/2} \cos \omega \right\} \quad (1)$$

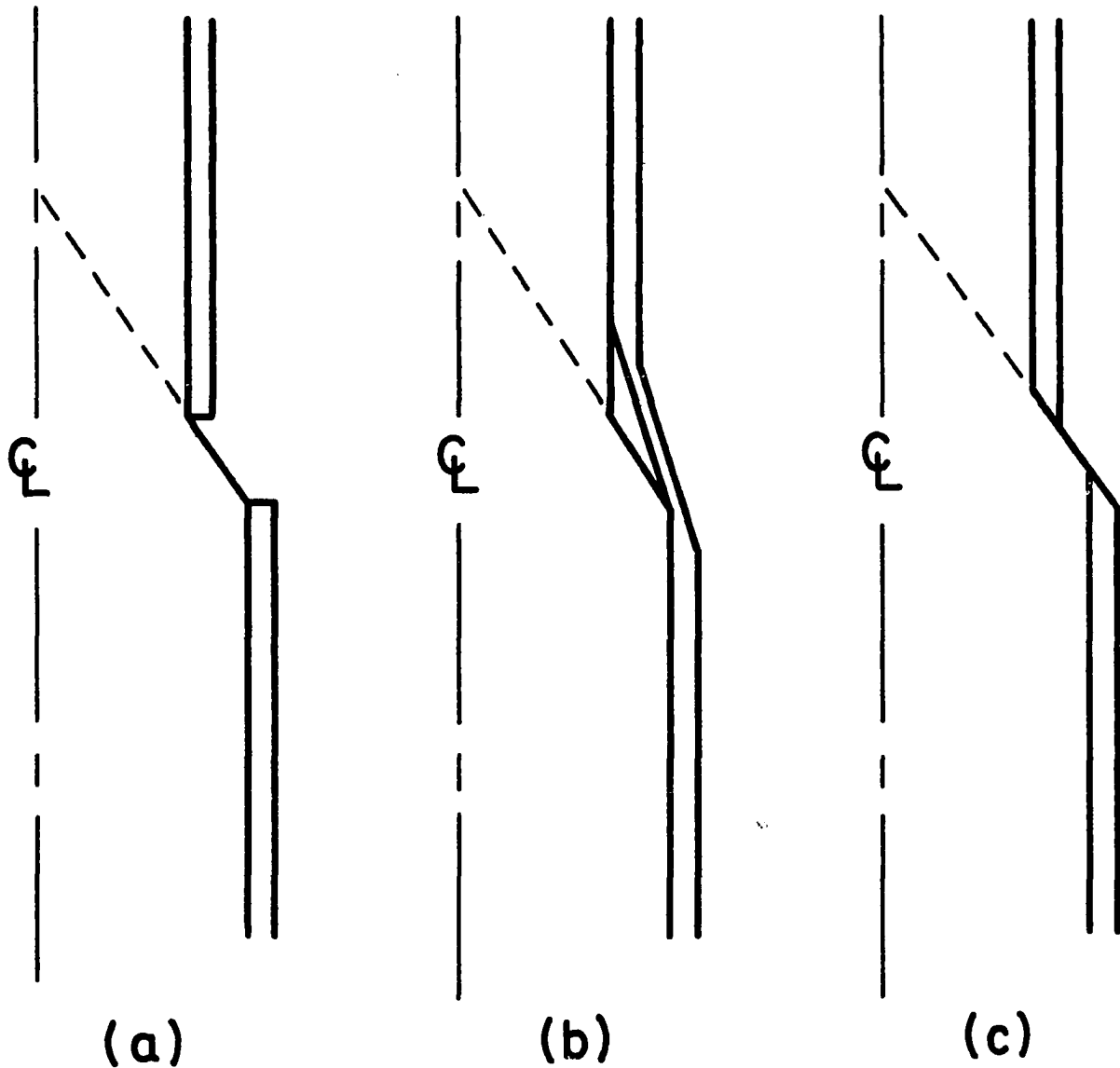


FIG. 10- Schematic diagrams of ways in which a film may accommodate slip in the substrate: (a) Film cracks along slip traces; (b) Film is initially detached without cracking; (c) Film shears off.

$$\cos \omega = (1/1+\epsilon) \left(1 + \cos \phi \left\{ \left[(1+\epsilon)^2 - \sin^2 \phi \right]^{1/2} - \cos \phi \right\} \right) \quad (2)$$

$$\sigma = E_c \left\{ \left[\frac{\epsilon}{0.38(1-K)} \right] (t/\alpha)^{1/2} \sin \omega \right\} \quad (3)$$

$$\sin \omega = \left[\frac{\sin \phi}{(1+\epsilon)} \right] \left\{ \left[(1+\epsilon)^2 - \sin^2 \phi \right]^{1/2} - \cos \phi \right\} \quad (4)$$

where λ and σ are shear and normal stresses developed at the coating-substrate interface due to the slip step. The other parameters that appear in the above equations are defined as follows:

- E_c = Young's Modulus of the coating
- ϵ = Substrate strain
- ν = Poisson's ratio for the coating
- t = Coating thickness
- α = Thickness of the interface layer (about 50 Å)
- ϕ = The angle between the slip plane and the surface
- K = A dimensionless parameter with value between 0 and 1

Equations (1) and (3) show that the film thickness, t , influences both λ and σ . Thus the thicker the film, the higher the normal and shear stresses at the slip steps due to the substrate strain. Very thick oxide coatings should therefore, tend to detach at the slip steps, provided that the strain required to produce λ_c and σ_c is not higher than the fracture strain of the coating, ϵ_f . In the case of the oxide-aluminum system, as the coating thickness increased, the coating suppressed surface slip. Direct evidence of this phenomenon will be presented in part II of this paper. Thus, with thick coatings the surface slip (steps) amounted to very mild surface undulations, even after considerable amount of deformation (see Figure 5). Thick anodic coatings accommodated these surface undulations without detachment at the slip steps (see Figure 6). Transverse*

*Although these cracks are not always perpendicular to the tensile axis, as discussed in the previous section, they will be referred to as transverse cracks.

cracking occurred when the substrate strain exceeded the fracture strain of the coating.

In the case of thin films, high substrate strains are required to produce stresses equal to the λ_c and σ_c . It is quite likely that these strains would surpass the fracture strain, ϵ_f , of the coating. The coating will then fracture at the slip steps. Thus, thin anodic films, $t \leq 900 \text{ \AA}$, fractured at the slip steps as shown in Figure 11, separating the film into strips. Transverse cracking then occurred according to the stress relaxation in these strips, the angle between the slip trace and the tensile axis, and the localized strains developed due to further deformation of the substrate.

Returning to Figure 8, we find extensive transverse cracking near the slip vector, Figure 8e, where the coating was subjected to the maximum tensile strain (22). At position D, Figures 8d and 11a, the slip steps are nearly perpendicular to the tensile axis so that the fracture at the slip steps was equivalent to transverse cracking. At 90° to position D, Figure 8a, the coating was subjected to maximum compressive circumferential strains (22), as evidenced by the film buckling. Thus, the local tensile strain was reduced. No transverse cracks were developed up to a substrate strain of 0.185. Such transverse cracks would have developed, had the specimen been strained further. Here, one should note that for thicker coatings, i.e., lower fracture strains, such cracks did appear at the equivalent position at much lower substrate strains, as shown in Figure 7.

At positions in between these two extremes the extent of transverse cracking increased as one approached the slip vector, as shown in Figures 8b and 8c.

Summary:

The fracture characteristics of the anodic coating as a function of the coating thickness were investigated. The fracture strain of the anodic coatings formed on aluminum single and polycrystalline specimens decreased as the coating thickness was increased. The origin of the observed decrease in the fracture strain as a function of thickness could

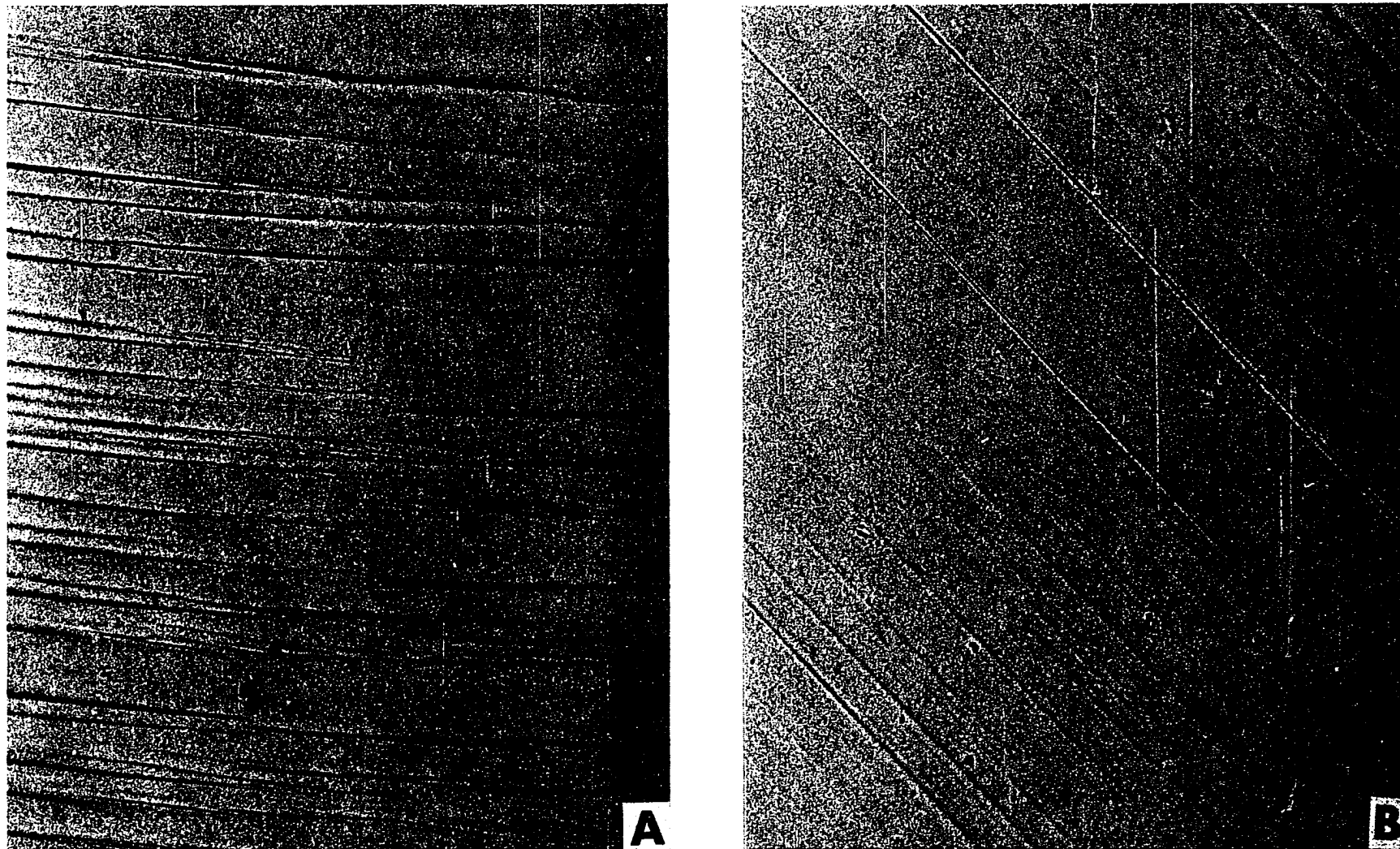


FIG. 11- Appearance of the slip steps at the edge (A) and screw (B) position of specimen R-7-5, covered with 300 Å thick anodic film, after 4% substrate elongation.
500X

not be directly determined but might have been the result of structural changes as the thickness increased.

The magnitude of the coating fracture strain relative to the substrate strain was measured in situ. Stress analysis applied to the coating-crystal system indicated that the coatings were under the influence of a system of biaxial stresses. The biaxial stress condition could explain why fracture strain measurements made directly on the separated films had higher values than the measurements made in situ (24). Because of the interaction of coating and substrate, study of the behavior of anodic coatings in isolation appears to be of limited value in determining their characteristics in composite systems.

The fracture mode of the anodic coatings was also investigated. Of the five possible mechanisms by which the film could accommodate substrate deformation, i.e., fracture at the slip steps, transverse cracks, film buckling, interfacial shear and detachment, the first two (with thin and thick films) were the dominant mechanisms during the initial stages of deformation. Film buckling required much higher substrate deformation to achieve the necessary circumferential contraction. Interfacial shear suggested elsewhere (23) will be considered in part II.

Coatings thicker than 1350 \AA accommodated substrate strain by transverse cracks. The angle between the transverse cracks and the tensile axis of the single crystal specimen could be predicted from the specimen geometry and the orientation of the crystal.

Coatings with thicknesses less than 900 \AA fractured at the slip steps, separating the film into strips. Transverse cracking then took place as demanded by the localized substrate strains, which were in turn influenced by the position of the surface relative to the slip vector.

The transition in the mode of fracture as a function of coating thickness had been predicted previously (31) based on equations (1) and (3) presented in this section. This investigation has presented the first quantitative data on the subject.

II - SURFACE DAMAGE

The damage induced by the anodic coating on the aluminum surface when it fractures will now be considered. As described earlier, transverse cracking occurred until the crack density reached a limiting value after which (Figure 12) further deformation merely opened the existing cracks. This observation is in agreement with the crack density data obtained by Edeleanu and Law (23) who attributed this phenomenon to the "inter-phase slip". An alternative explanation is to assume that once elastic relaxation due to cracking of the film inhibits the formation of new cracks, preferential deformation occurs in the substrate beneath and immediately adjacent to existing cracks.

In order to test this hypothesis the following experiment was performed. A square single crystal was anodized at 30 volts (450 Å thickness) and deformed until extensive cracking and film buckling had taken place. Figure 13a shows one face of this specimen. Note that the mode of film deformation on this face is a mixture of fracture at the slip steps and transverse cracking. Figure 13b shows the surface after the anodic film was removed in the oxide stripping solution. The transverse markings are grooves in the substrate brought about by the preferential deformation of substrate underneath the cracks.

A similar experiment was performed using a square crystal and 3000 Å anodic coating. The result is shown in Figure 14 a and b. The only notable difference in the two photomicrographs was the absence of interference fringes underneath the folds in Figure 14b. The extent of deformation under the cracks can be appreciated by their interaction with the two micro-hardness indentation marks. Preferential deformation has also taken place under the detached coating where film buckling had occurred. Comparison of Figures 13b and 14b shows (as expected) that the extent of preferential deformation is much more severe in the case of thick anodic coatings.

The thick anodic coating has suppressed slip at the surface as noted in Figure 14b. However, the rough striations are evidence of surface slip under the buckles. This is further illustrated

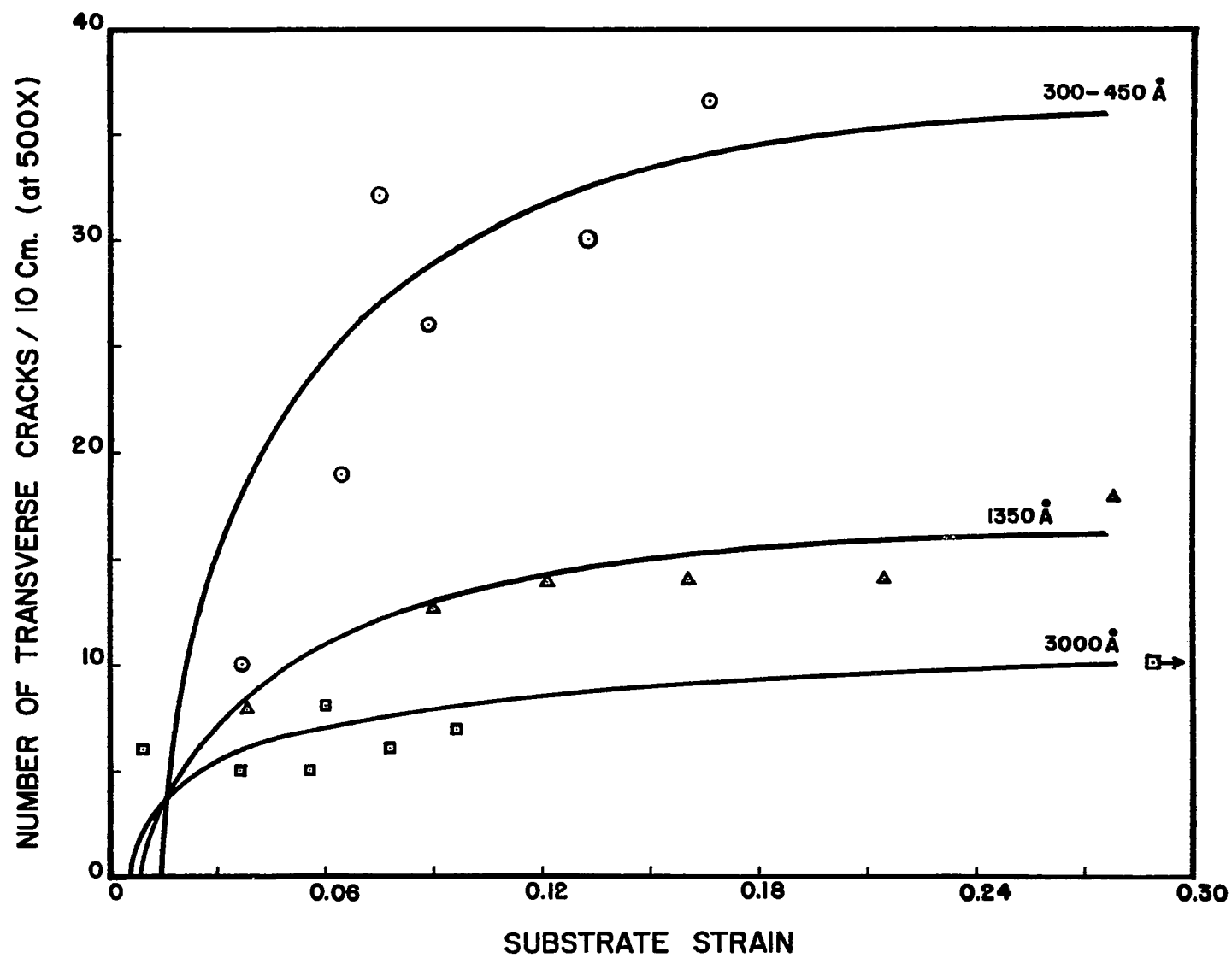


FIG. 12- Density of transverse crack v.s. substrate strain for anodic films of different thicknesses.

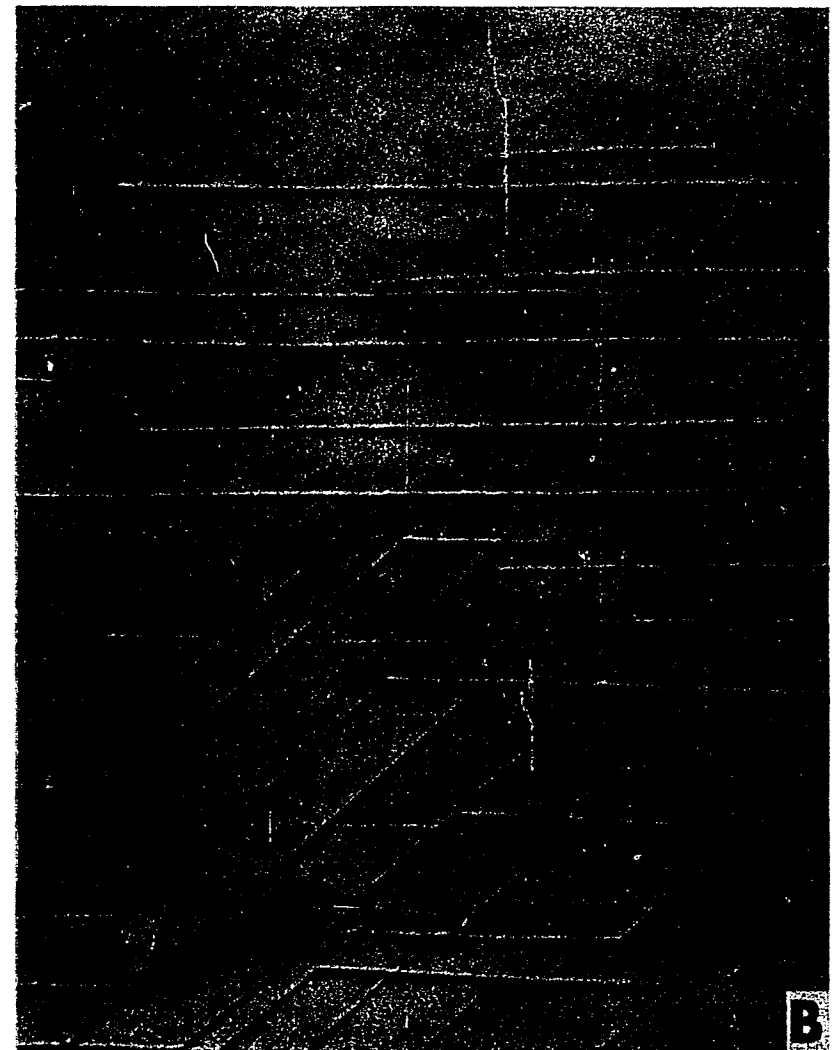


FIG. 13- Appearance of the surface of a square crystal covered with 450 Å thick anodic coating, strained 7.5%, before (A) and after (B) the coating was stripped off.

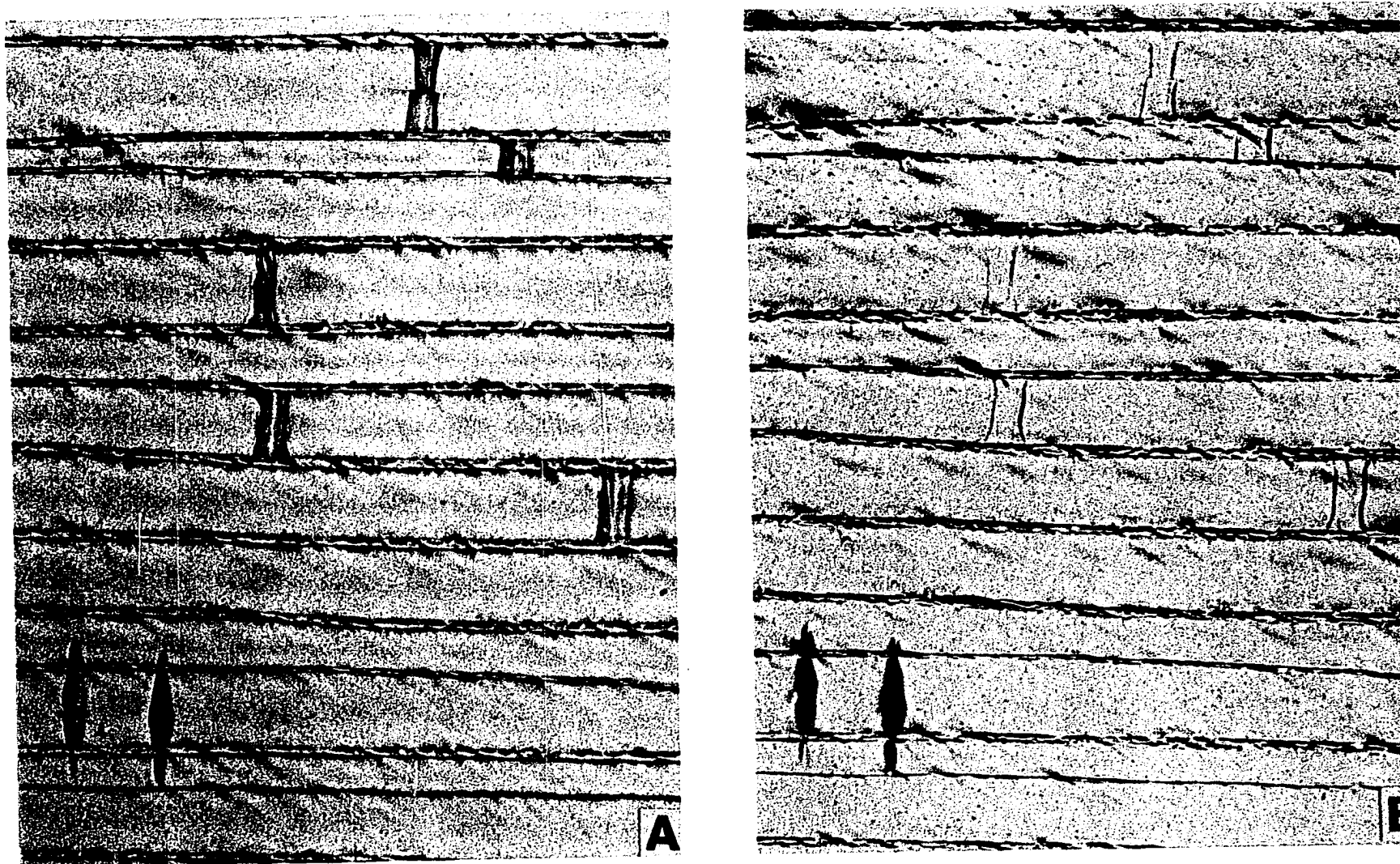


FIG. 14- Appearance of the surface of specimen 3-4A, covered with 3000 Å thick anodic coating and strained 10%, before (A) and after (B) the coating was stripped off.

by the diagonal lines in the higher magnification photomicrograph of Figure 15a. Continued deformation of the stripped crystal produced the well defined coarse slip lines shown in Figure 15b, in contrast to the fine slip lines that were found underneath the thin anodic coating in Figure 13b.

Discussion:

From the foregoing argument, it may be deduced that the magnitude of surface deformation depends upon the density of cracks and the state of stress underneath the coating, between the cracks. Because the film cracks from the free surface inward the strain in the anodized film, immediately after it cracks, must be reduced everywhere within the thickness of the coating (relaxation at the common layer between the substrate and the coating occurs later). This is illustrated schematically in Figure 16a. The resultant stress distribution (32) is shown in Figure 16b. For any point at the edge of the cracks, both the residual stress and the applied stress in the direction of σ_1 are reduced to zero. For other points within the coating, these stresses are reduced relative to σ_1 . The stress in the coating between two cracks can be represented (31) as shown in Figure 16c by:

$$\sigma_1(x) = \sigma_f \left[1 - g \left(\frac{1}{x} + \frac{1}{d_o - x} \right) \right] \quad (1)$$

where g is a parameter with dimension of length and σ_f is the fracture stress of the coating. The relation between g , the crack width w , and the coating thickness t is:

$$g = x/2 = k \sqrt{t} \quad (2)$$

where k is a constant that can be determined experimentally. Thus the stress midway between two cracks at $x = d_o/2$ can be written:

$$\sigma_c(d_o/2) = \sigma_f [1 - 4k/t/d_o] \quad (3)$$

where σ_c is the stress in the coating.

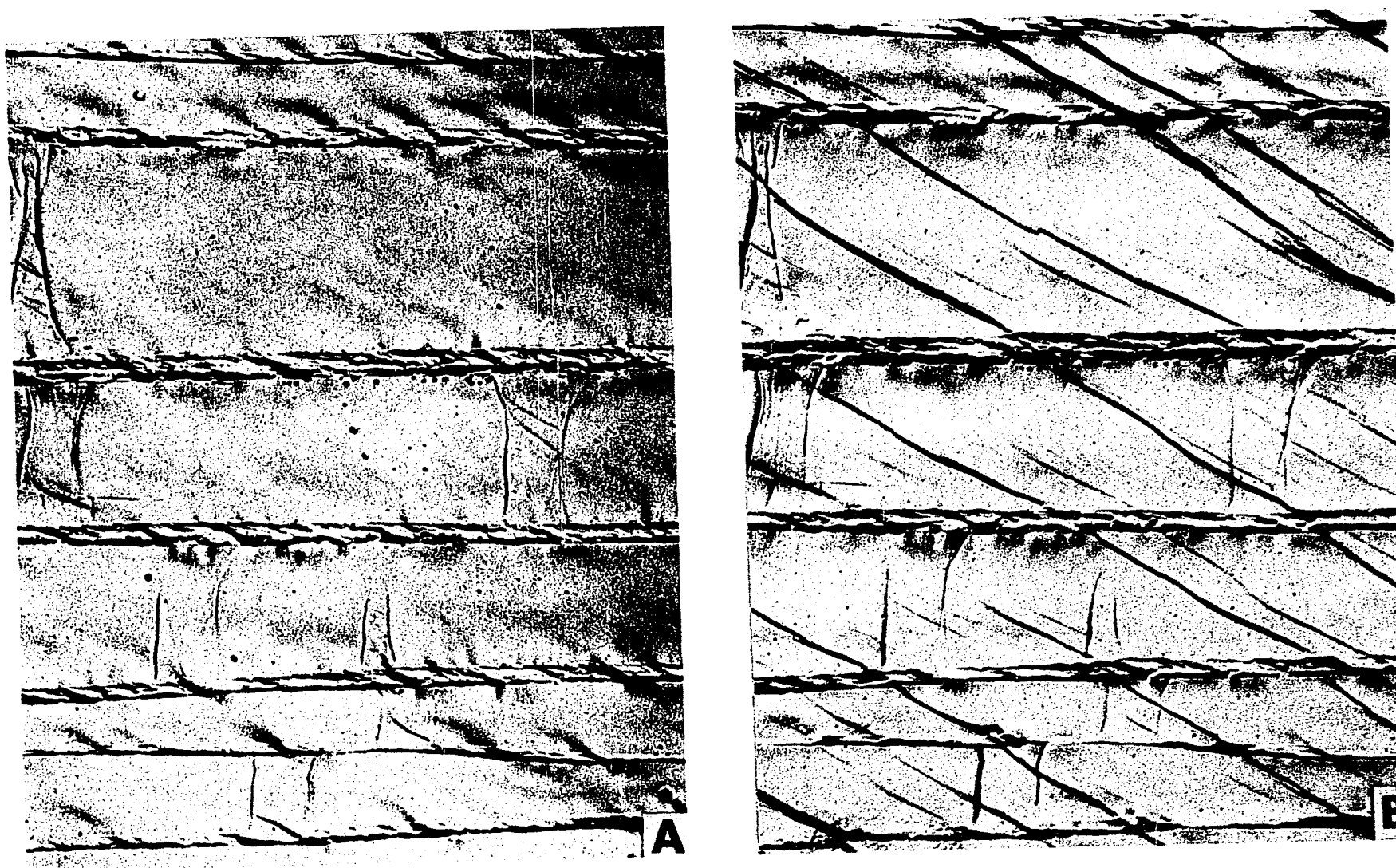


FIG. 15- Appearance of the surface of specimen 3-4A, covered with 3000 Å thick anodic film and strained 10%, after the coating was stripped off (A), and upon 3% further deformation (B).

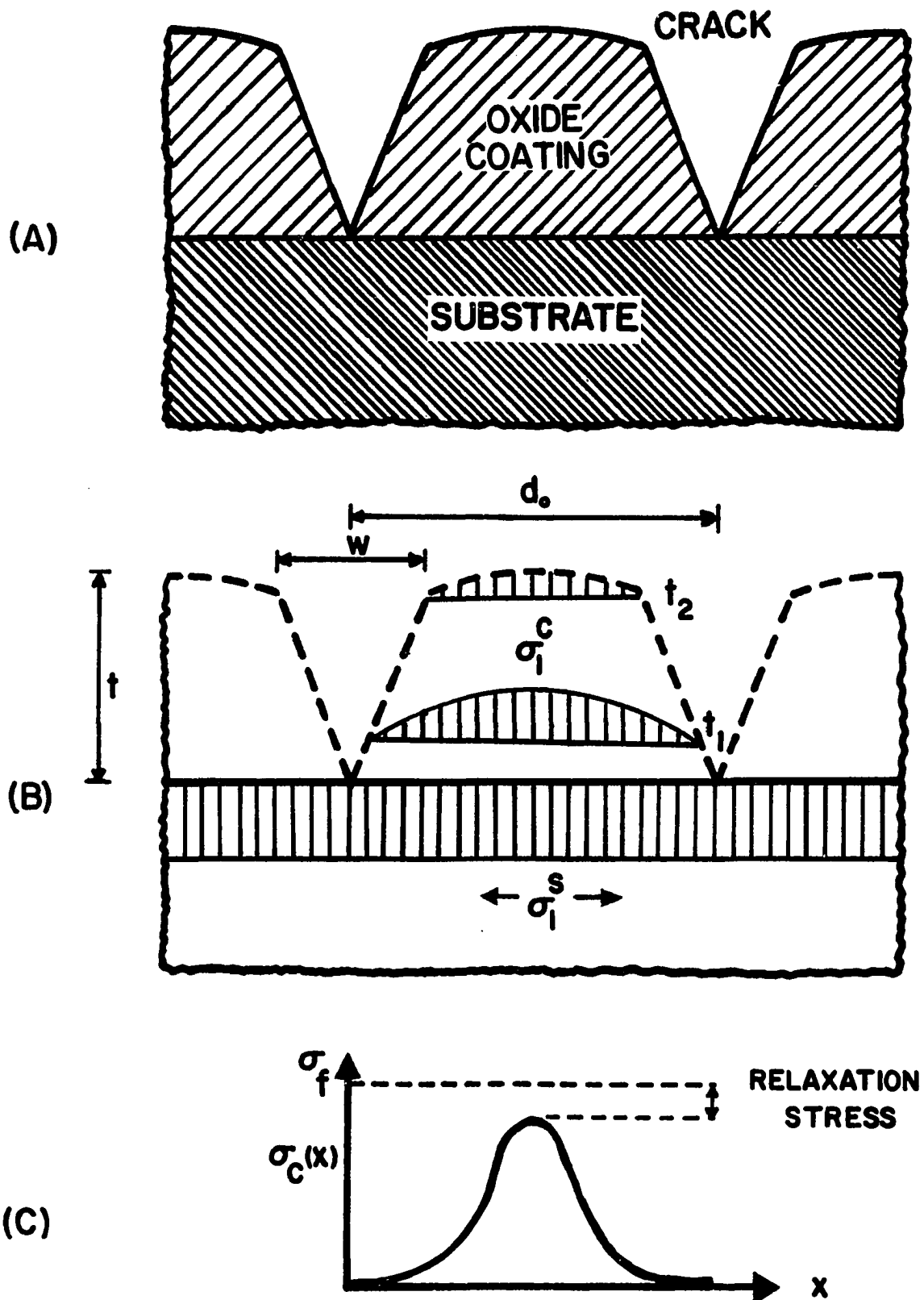


FIG. 16- Stress distribution in the coating, between two interacting transverse cracks.

As the deformation is continued additional cracks are produced when $\sigma_c = \sigma_f$ at $x = d_o/4, d_o/8 \dots$ etc. The crack multiplication occurs according to:

$$\ln \epsilon / \epsilon_o = 4k \sqrt{f} \left(\frac{1}{d} - \frac{1}{d_o} \right) \quad (4)$$

where ϵ_o and d_o are the substrate strain and crack spacing for two interacting cracks, d being the crack spacing at strain:

$$\epsilon = \epsilon_o + \Delta\epsilon \quad (5)$$

An interesting consequence of equation (4) is that it shows the saturation crack spacing is a function of coating thickness, and the saturation crack spacing is larger, the thicker the coating in agreement with the data of Figure 12a. Equation (3) indicates that the peak stress between two cracks is lower, and thus the extent of preferential deformation higher, the thicker the coating. Again in agreement with the experimental observation reported with respect to Figures 13 and 14.

Summary:

The deformation caused by fracture of anodic coating on the surface of the aluminum single crystal, was considered in part II of this study.

The crack density, and important parameter in the study of the surface damage, as a function of coating thickness and substrate strain was determined. The density of transverse cracks increased as the coating thickness was decreased.

When transverse cracking occurred, the crack density reached a plateau and further deformation merely opened the existing cracks. The equilibrium crack density was a function of the coating thickness. Consideration of this phenomenon indicated that elastic relaxation of the film subsequent to cracking inhibited the formation of new cracks. Further deformation of the film-substrate system induced preferential deformation of the substrate in the existing cracks.

Metallographic examination of the anodized single crystal specimens, which were deformed until cracking and film buckling had taken place, showed that suppression of surface slip and preferential deformation of the substrate in the cracks had occurred. Both thick and thin films induced preferential deformation where transverse cracking had occurred. Thick coatings had lower crack densities and consequently greater deformation at the cracks than thin coatings.

III - THE EFFECTS OF ANODIC FILMS ON THE PLASTIC DEFORMATION OF ALUMINUM SINGLE CRYSTALS

STAGE I

Having considered in some detail the behavior of anodic coatings during deformation, their influence upon the deformation behavior of the substrate may now be considered. A parallel exists with previous work (14) where metallic coatings on copper crystal substrates were used. In this work preferential deformation at cracks resulting from film fracture seemed to be the critical factor in producing the film strengthening effects. Also, significant film strengthening was always accompanied by film cracking either prior to or during the deformation of the substrate and was the result of residual stresses in the coating.

In view of these findings, it is appropriate to consider the effect of anodic films on the stage I parameters of aluminum single crystals as a two-step process:

- (a) Factors that influence the mechanical behavior of the substrate prior to the fracture of anodic films. These include the state of residual stress in the coating and the effectiveness of the coating as a barrier to the egress of dislocations.
- (b) Factors that influence the mechanical properties of the substrate during and subsequent to the fracture of anodic film. This group includes the mode of fracture, and the introduction of excess dislocations at the surface due to cracking and relaxation of the coating.

In this section the relative contribution of each of the above processes to changes in mechanical behavior of substrate will be discussed.

Using the information from previous sections it may be concluded that thin anodic coatings (high fracture strains) should exert their influence mainly by processes mentioned in (a).

On the other hand, thick anodic coatings (low fracture strains) should influence the mechanical behavior of the substrate through both (a) and (b) processes.

It should then be possible to assess the relative importance of the different factors by studying the changes of stress-strain parameters of aluminum single crystals during stage I of deformation as a function of anodic coating thickness.

Considering the previous discussion regarding the state of residual stresses in the anodic films (25,27), their influence upon the substrate prior to film cracking should be especially important.

Results:

The stress-strain parameters of aluminum single crystals coated with anodic films of different thicknesses defined according to Figure 17 and determined by the methods of Appendix B and C are shown in Tables 3 and 4. As may be noted, there is some scatter in the measured values of the parameters for crystals grown from different seeds, but of similar orientations. However the reproducibility of the data among the specimens cut from the same crystal was adequate. The only parameter that showed considerable variation was the critical resolved shear stress, τ_o , which was strongly influenced by the condition of specimen surface. This may be illustrated by comparisons of data from specimens R-7-3 and R-7-4. The lower flow stress of R-7-4 was due to the grooves left on the surface by the thick oxide layer formed during the growth from the melt. To make meaningful comparisons of the data, the changes in various parameters produced by the anodized coating were measured relative to an uncoated specimen of the same crystal. The relative changes in the stress-strain parameters during Stage I are shown in Table 5 as a function of coating thickness. The stress-strain curves are presented in Figures 18 to 23.

To investigate the effects of the state of residual stress in the anodic films, data were obtained on specimens anodized at high (2 ma/cm^2) and low (0.2 ma/cm^2) formation rates. The formation rate was, therefore, included in Table 5. Henceforth, it will be

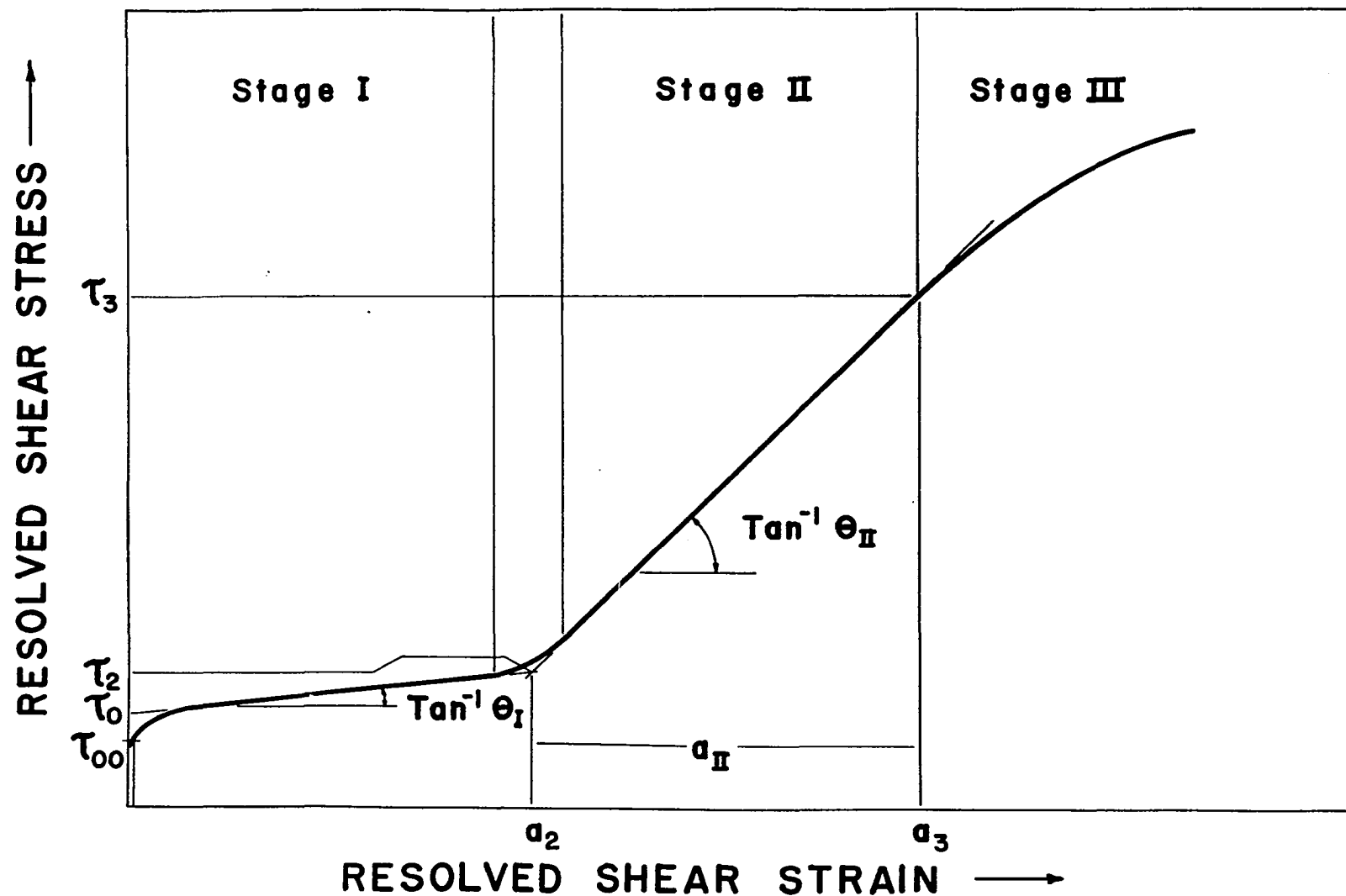


FIG. 17- Conventions used in determining the stress-strain parameters of aluminum single crystals.

TABLE III
STRESS-STRAIN PARAMETERS OF THE SPECIMENS
STAGE I

Specimen Designation	Coating Thickness \bar{A}	Residual* Stress	τ_o g/mm^2	Θ_1 g/mm^2	α_2 %	τ_2 g/mm^2
R-6-1	1350	T	52.648	3097.69	1.989	111.031
R-6-2	450	C	49.746	2819.64	2.618	130.490
R-6-5	clean	-	39.136	2319.74	2.329	100.030
R-7-3	clean	-	48.907	2507.13	2.506	106.850
R-7-4	clean	-	40.004	2727.87	2.635	110.480
R-7-5	300	C	47.054	3084.55	2.567	128.350
R-11-2	clean	-	48.045	2037.96	2.570	102.060
R-11-3	1350	C	53.304	2683.32	3.270	141.760
R-15-1	3000	C	36.358	3128.48	3.004	128.600
R-15-2	clean	-	33.881	1980.00	1.908	80.710
R-16-2	450	T	41.722	2147.41	2.491	116.630
R-16-3	3000	T	60.175	3851.82	1.987	136.770
R-16-4	clean	-	44.902	1851.46	2.610	104.350

*T- Tensile residual stress, formation rate: 2 ma/cm^2 .

C- Compressive residual stress, formation rate: 0.2 ma/cm^2 .

TABLE 4
STRESS-STRAIN PARAMETERS OF THE SPECIMENS USED
STAGE II

Specimen Designation	Coating Thickness Å	Residual* Stress	Θ_{II} g/mm ²	α_3 %	τ_3 g/mm ²
R-6-1	1350	T	6054.24	5.408	303.88
R-6-2	450	C	4513.94	8.020	367.46
R-6-5	clean	-	5220.38	7.230	339.49
R-7-3	clean	-	4259.89	7.440	317.61
R-7-4	clean	-	4459.75	8.567	370.85
R-7-5	300	C	4024.74	6.753	296.00
R-11-2	clean	-	4370.41	7.370	301.23
R-11-3	1350	C	3559.57	10.077	374.26
R-15-1	3000	C	6287.66	5.092	251.02
R-15-2	clean	-	5531.68	5.290	257.08
R-16-2	450	T	5483.81	6.980	314.52
R-16-3	3000	T	5170.65	6.420	355.27
R-16-4	clean	-	4616.51	7.540	314.18

*T-Tensile residual stress, formation rate: 2 ma/cm².

C- Compressive residual stress, formation rate: 0.2 ma/cm².

TABLE 5
CHANGES IN THE STAGE I STRESS-STRAIN PARAMETERS OF ALUMINUM SINGLE
CRYSTALS DUE TO ANODIC FILMS OF DIFFERENT THICKNESS AND STATE OF
RESIDUAL STRESS

Specimen Designation	Coating Thickness \AA	Residual Stress*	$\Delta\alpha_2$ %	$\Delta\Theta_1$ g/mm^2	$\Delta\tau_2$ g/mm^2
R-16-2	450	T	-0.12	296	12.3
R-6-1	1350	T	-0.34	778	23.2
R-16-3	3000	T	-0.62	2000	32.4
R-7-5	300	C	+0.07	367	25.1
R-6-2	450	C	+0.19	499	26.7
R-11-3	1350	C	+0.69	645	39.7
R-15-1	3000	C	+1.10	1148	39.6

*T-Tensile residual stress, formation rate: 2 ma/cm^2 .

C- Compressive residual stress, formation rate: 0.2 ma/cm^2 .

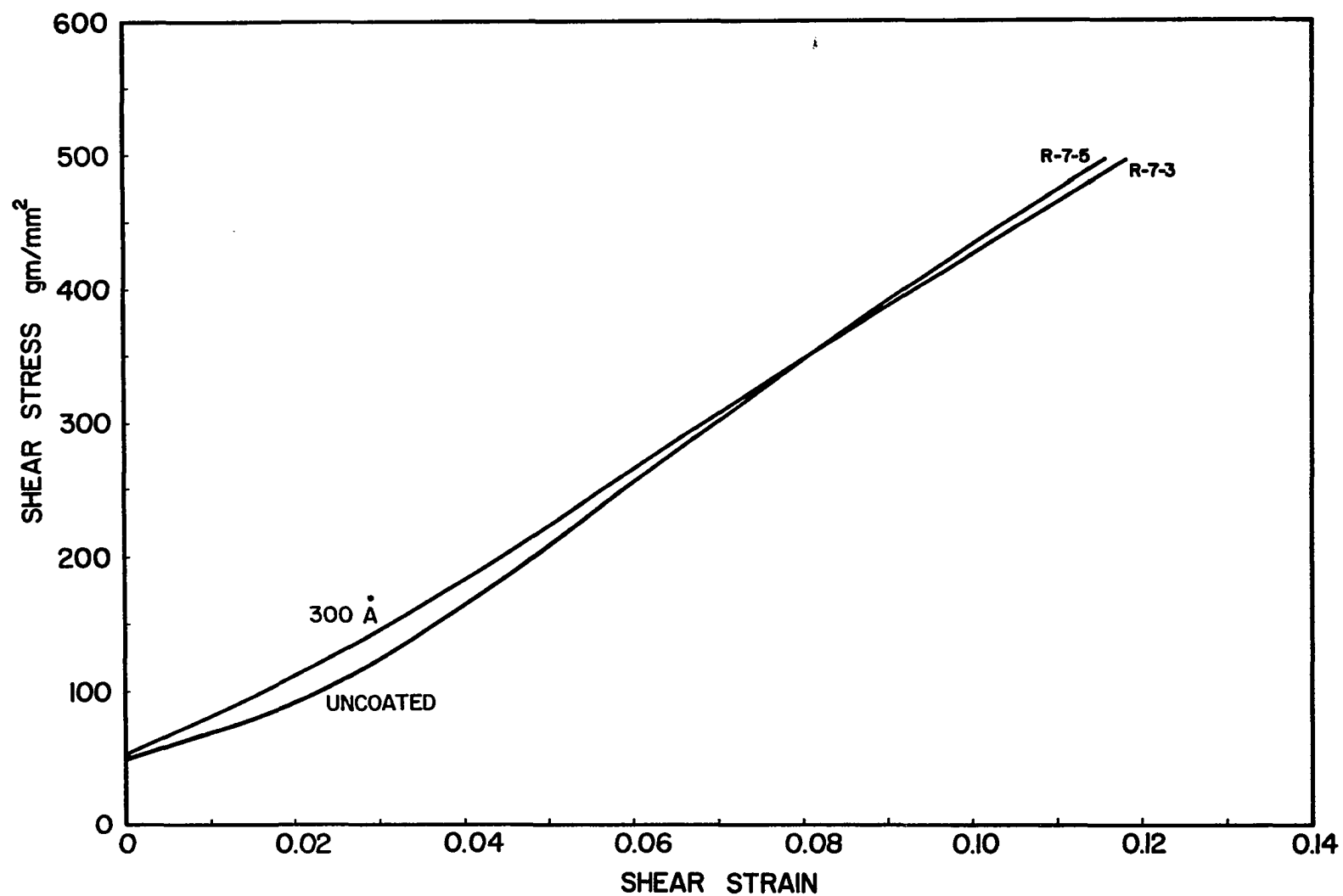


FIG. 18- Stress-strain curves for coated and uncoated aluminum single crystals indicating the effect of 300 Å thick anodic film with compressive residual stress.

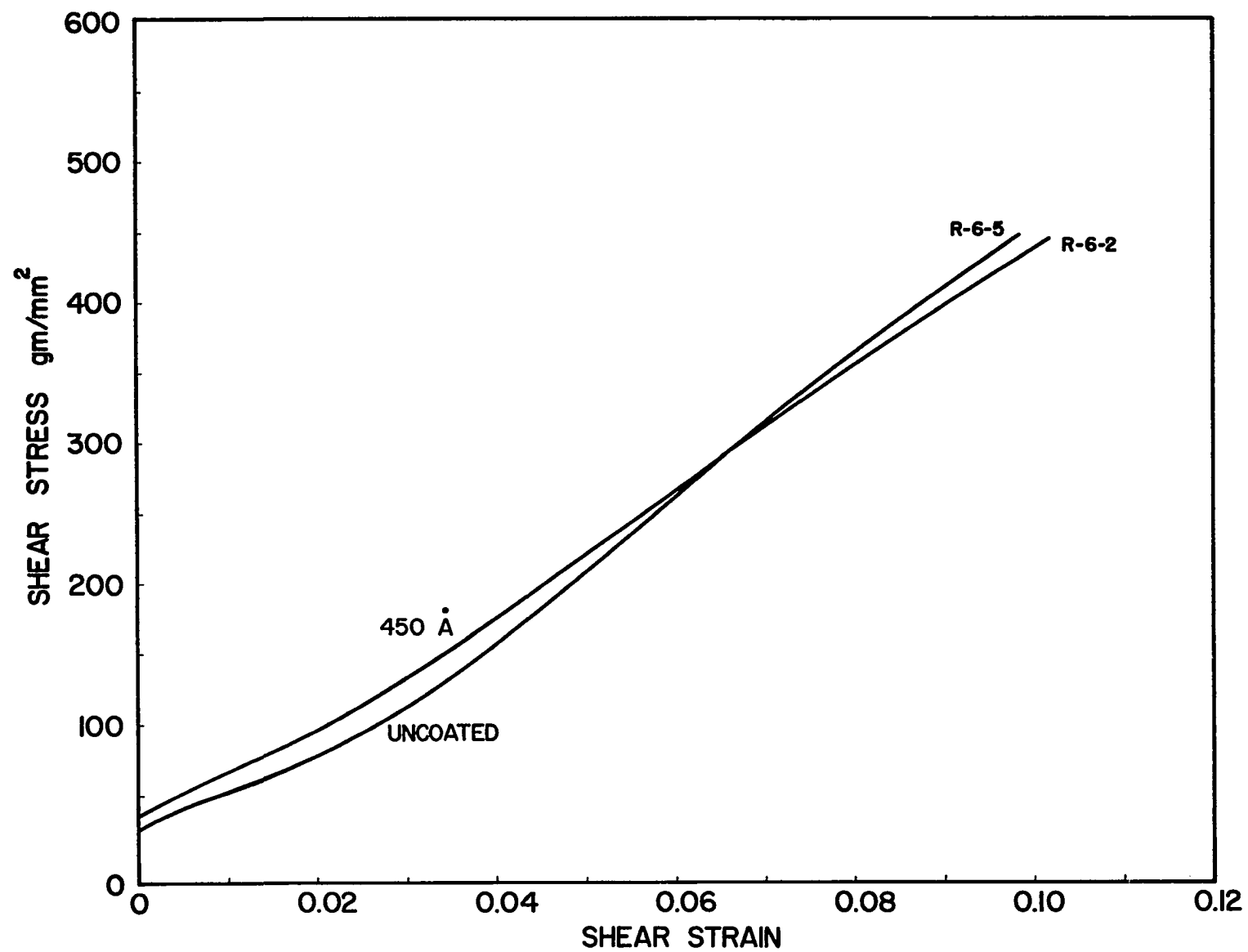


FIG. 19- Stress-strain curves for coated and uncoated aluminum single crystals indicating the effect of 450 Å thick anodic film with compressive residual stress.

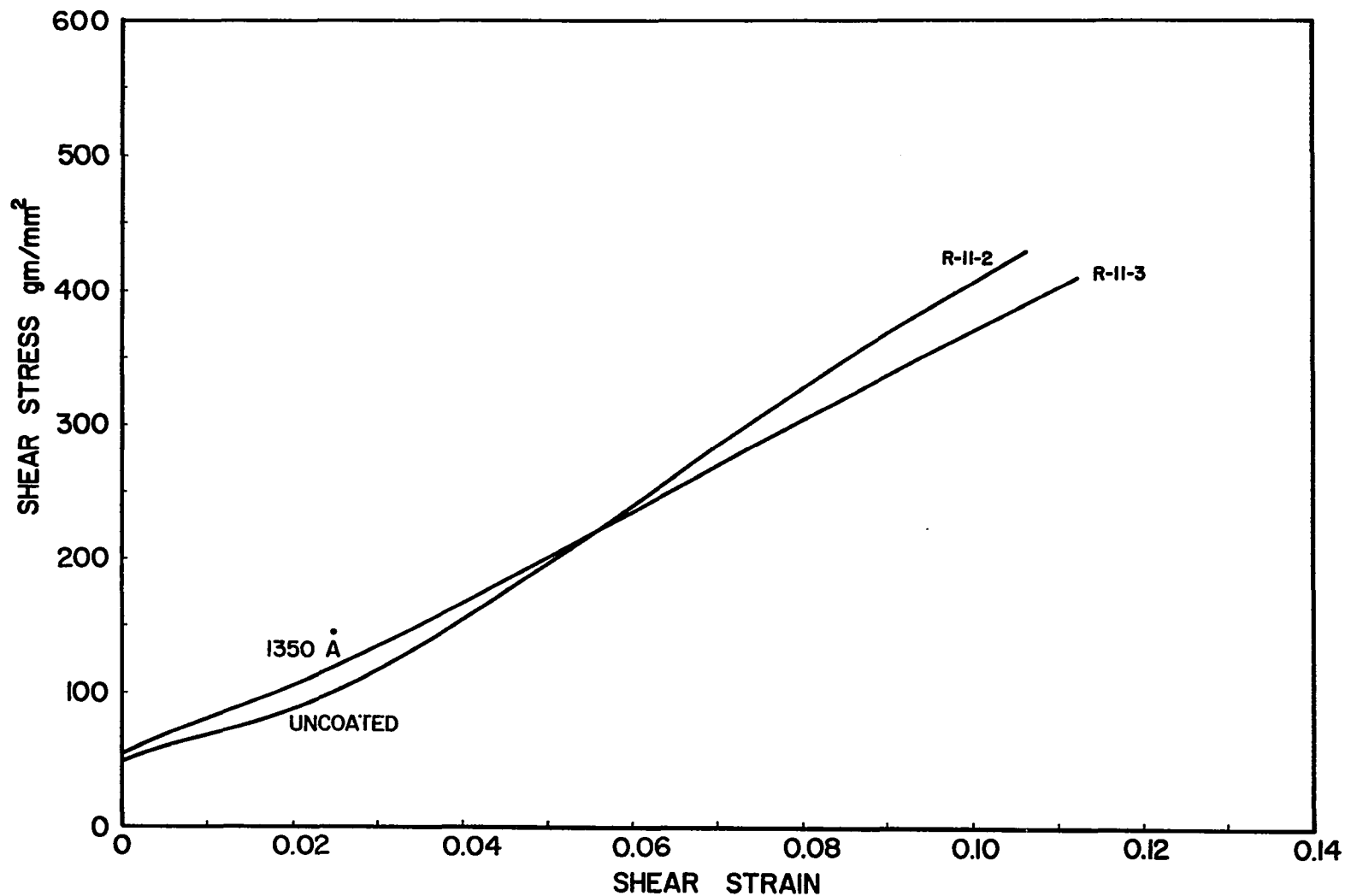


FIG. 20- Stress-strain curves for coated and uncoated aluminum single crystals indicating the effect of 1350 Å thick anodic film with compressive residual stress.

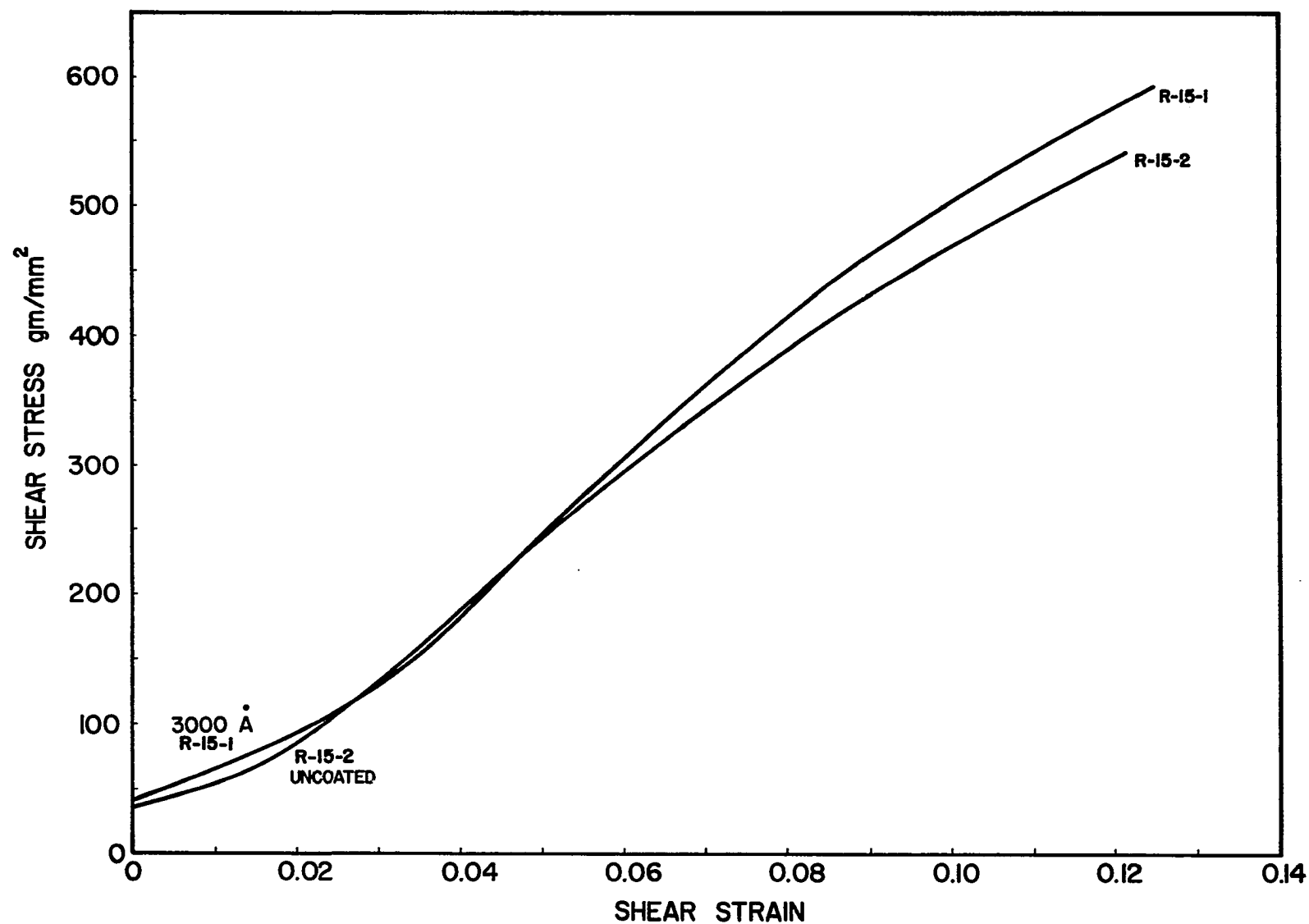


FIG. 21- Stress-strain curves for coated and uncoated aluminum single crystals indicating the effect of 3000 Å thick anodic film with compressive residual stress.

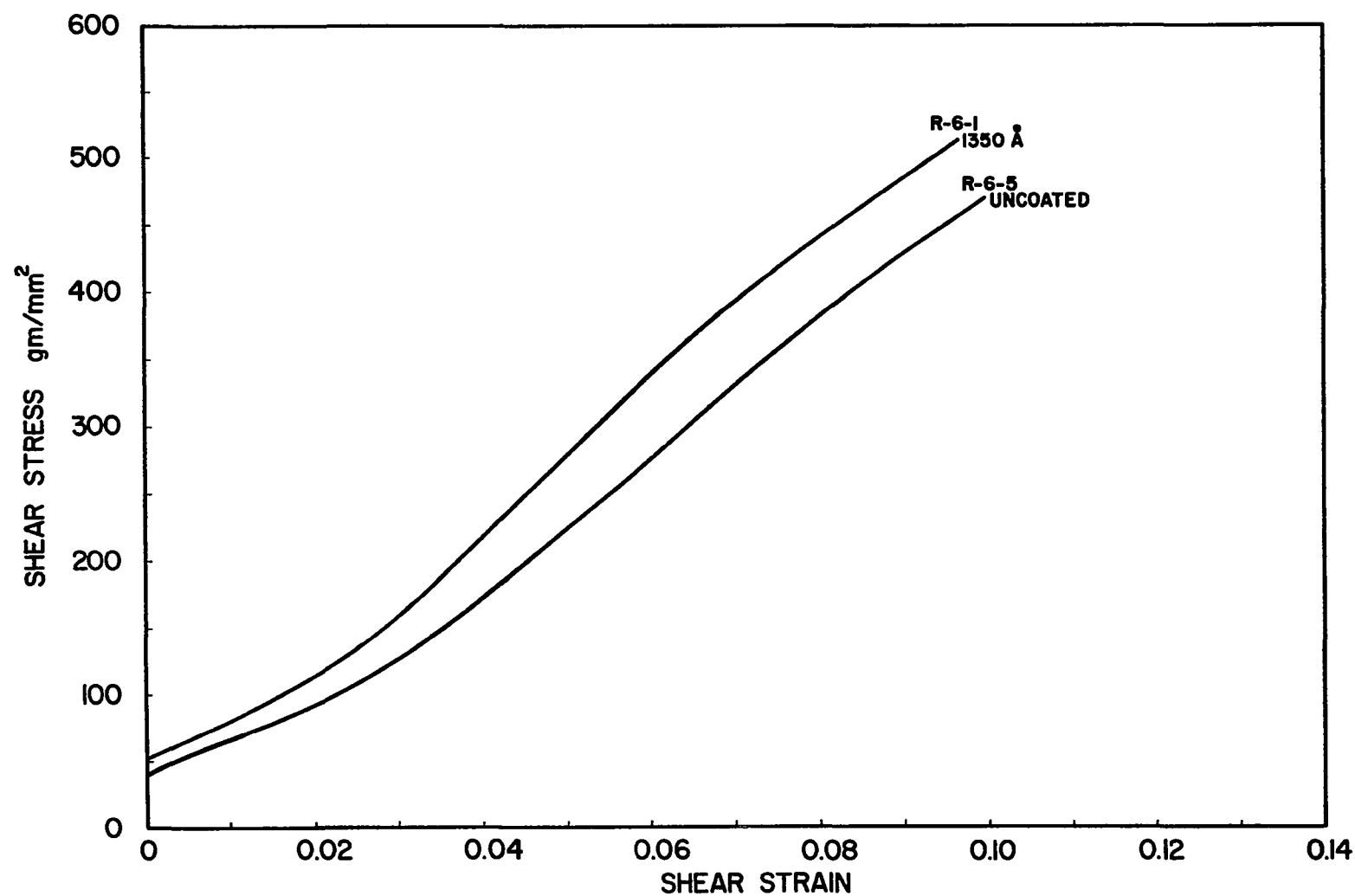


FIG. 22- Stress-strain curves for coated and uncoated aluminum single crystals indicating the effect of 1350 Å thick anodic film with tensile residual stress.

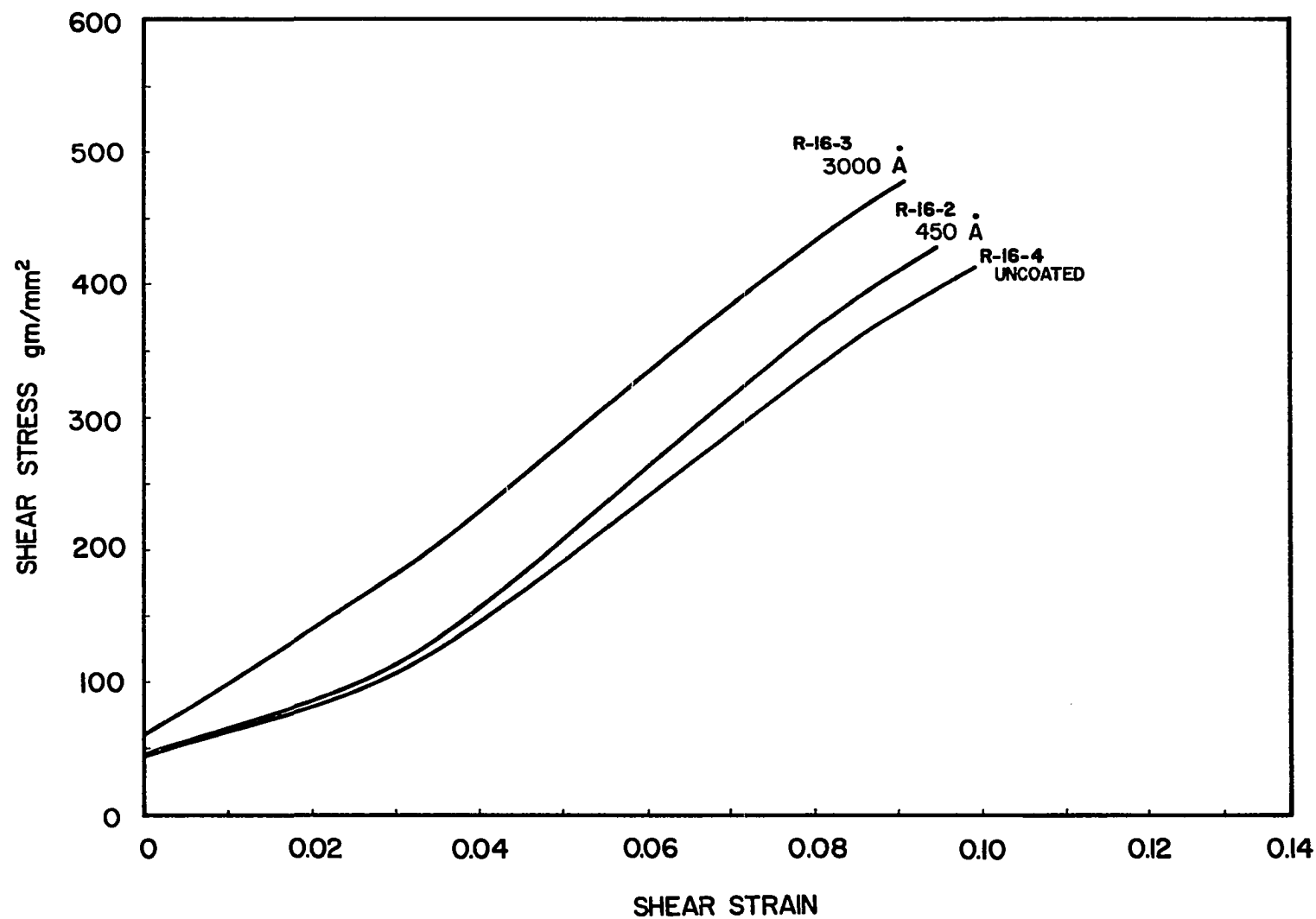


FIG. 23- Stress-strain curves for coated and uncoated aluminum single crystals indicating the effect of 450 Å and 3000 Å thick anodic films with tensile residual stress.

assumed that the anodic films formed at low formation rates are in compression while the films formed at high formation rates have high tensile residual stresses (according to our previous discussion).

In general, the critical resolved shear stress increased when the specimen was anodized. However, due to the large variation of flow stress among uncoated crystals, no relationship could be established. The other parameters of stage I, i.e., the duration of easy glide (a_2), the slope (Θ_1) and the stress at the start of stage II (τ_2), showed systematic changes with both the film thickness and the state of residual stress. Anodic films formed at low rates increased the extent of easy glide, a_2 , Θ_1 and τ_2 relative to uncoated crystals. Furthermore, the magnitude of these changes were larger for thicker coatings. On the other hand, coatings formed at high rates exhibited the expected behavior i.e., decrease in duration of stage I, a_2 , and increase in Θ_1 and τ_2 . Again, the effect was more pronounced for thicker coatings. Another feature of the specimens formed at low rates was that their stress-strain curves crossed those of their control tests. This is demonstrated in Figures 18 to 21. The stress-strain curve of a specimen having a 3000 Å coating crossed that of the uncoated curve twice as shown in Figure 21. This was due to the higher a_2 and lower Θ_{II} for all of the coatings, except the 3000 Å coating which had higher Θ_{II} .

Discussion:

Comparison of the tensile parameters of specimens having coatings formed at low rates with uncoated specimens indicate that the coatings had residual compressive stresses. The effect of anodic films with tensile residual stresses on the mechanical properties of aluminum single crystals are similar to the effects of chromium coatings on copper single crystals (32) and other electrodeposited metallic coatings having tensile residual stresses (14). The crossing of the stress-strain curves characteristic of anodic films with compressive residual stresses was also observed by Gilman and Read (33) for gold electrodeposited on zinc and by Takamura (5) for anodic films formed on aluminum. Gilman and Read attributed the effect to the orientation of the crystal while Takamura suggested

that the effect was due to the suppression of "bands of secondary slips" or kink bands by the surface films. It was believed that development of such kink bands caused intense work hardening; thus, their suppression resulted in work softening.

Johnson and Block (14) also produced stress-strain curves which crossed using electro-deposited gold coatings on copper crystals oriented for long easy glide. Their results, along with the data reported here, show that the effect is not due to specimen orientation as proposed by previous workers (5,33), since in each case the stress-strain curves of coated and uncoated specimens can either cross or diverge depending on the state of residual stress in the coating. It is also difficult to attribute the effect to suppression of kink bands since kinking does not occur to any great extent in copper crystals.

There is very little information in the literature concerning the effects of residual stresses in coatings on the mechanical properties of single crystal substrates. Data cited previously (14) and results here show that the main contribution of compressive residual stress is to increase the duration of easy glide. In this regard, it is interesting to note that Worzala and Robinson (34) showed that micropeening the surface of silver single crystals increased the duration of stage I. They explained the results in terms of activation of near surface sources. However, the introduction of compressive stresses at the surface may have been important. There is considerable evidence (35-39) that dislocation sources near the surface are activated very early in the process of plastic deformation. Hirsch (40) considers stage I to be the results of surface dislocation sources producing loops which move into the bulk. Easy glide ends when the ability of near surface sources to generate glide dislocations is exhausted by the back stress caused by pile-ups in the bulk. Pile-ups result from the interaction of glide dislocations with the grown-in forest of dislocations. This model of stage I agrees well with the experimental results (36,41).

The magnitude of the residual stress in the anodic coatings ($4-10 \text{ kg/mm}^2$) (24) is much higher than the flow stress (critical resolved shear stress) of aluminum single crystals ($0.03-0.06 \text{ kg./mm}^2$). The effect of coating can then be best represented as a highly

stressed surface. The presence of a compressively-stressed layer on the surface prior to tensile deformation can then facilitate the operation of the surface sources through the Bauschinger effect (42). By the same argument, the presence of tensile residual stress will produce the opposite effect. According to this model, one would expect a decrease in the duration of easy glide for a coating with tensile residual stress and an increase in the length of easy glide for coatings with compressive residual stresses, as shown by the data in Table 5.

The suppression of surface slip by the anodic films should result in higher back stress on the near-surface dislocation sources, only after a few dislocation loops have been generated. Therefore, further slip would be confined to either areas where film fracture has occurred along the slip lines, or by activation of shorter sources within the bulk. The second process will increase the slope of the stage I since higher stresses are required. Consequently, one would expect to observe coarse slip lines along the slip planes where the anodic coating had fractured, and fine slip underneath the coating. This was seen in Figure 13. Furthermore, it was observed that the blocking ability of coating increased as the coating thickness was increased. Thus, the contribution to flow stress due to this effect should also increase.

We may now discuss the factors that influence the mechanical properties of the substrate subsequent to the fracture of anodic coatings. Here it is important to assess the extent of the contribution made by these factors to the changes in the deformation parameters of stage I.

One must first consider the fracture strain of the coating relative to the stress-strain curve of the substrate to establish the strain at which the "surface damage" begins. Figures 24 and 25 show the tracing of load-potential-elongation curves for 3000 \AA and 300 \AA thick anodic coatings. The thick coating (3000 \AA), fractured quickly and saturation spacing was established within 0.5% extension. This is indicated by the sharp rise and the plateau of the potential curve in Figure 24. On the other hand, the fracture of thin coatings begins in stage II. Due to the mixed mode of fracture (i.e. transverse

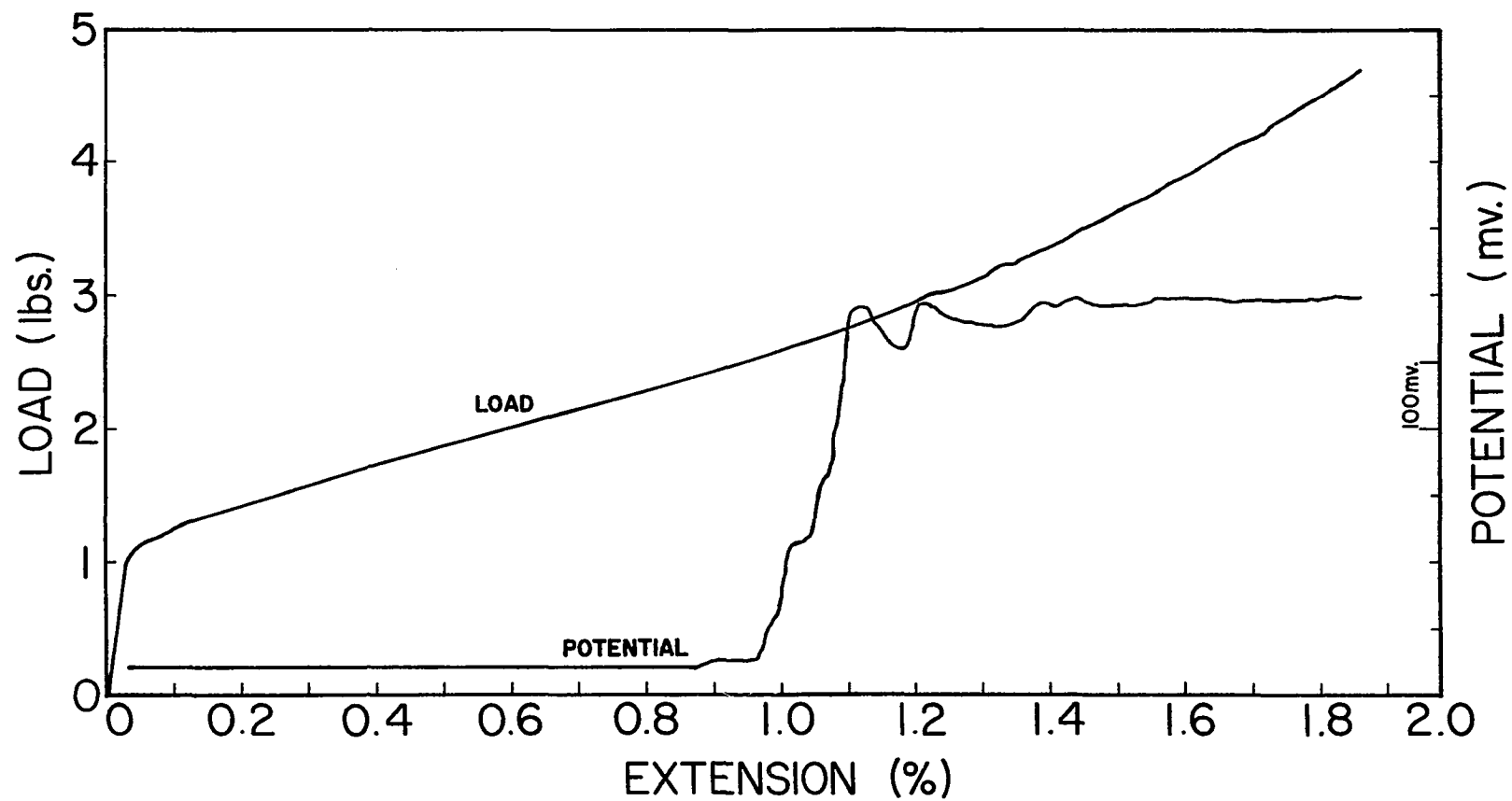


FIG. 24- Load-potential-extension curves for specimen R-15-1, coated with 3000 Å thick anodic film

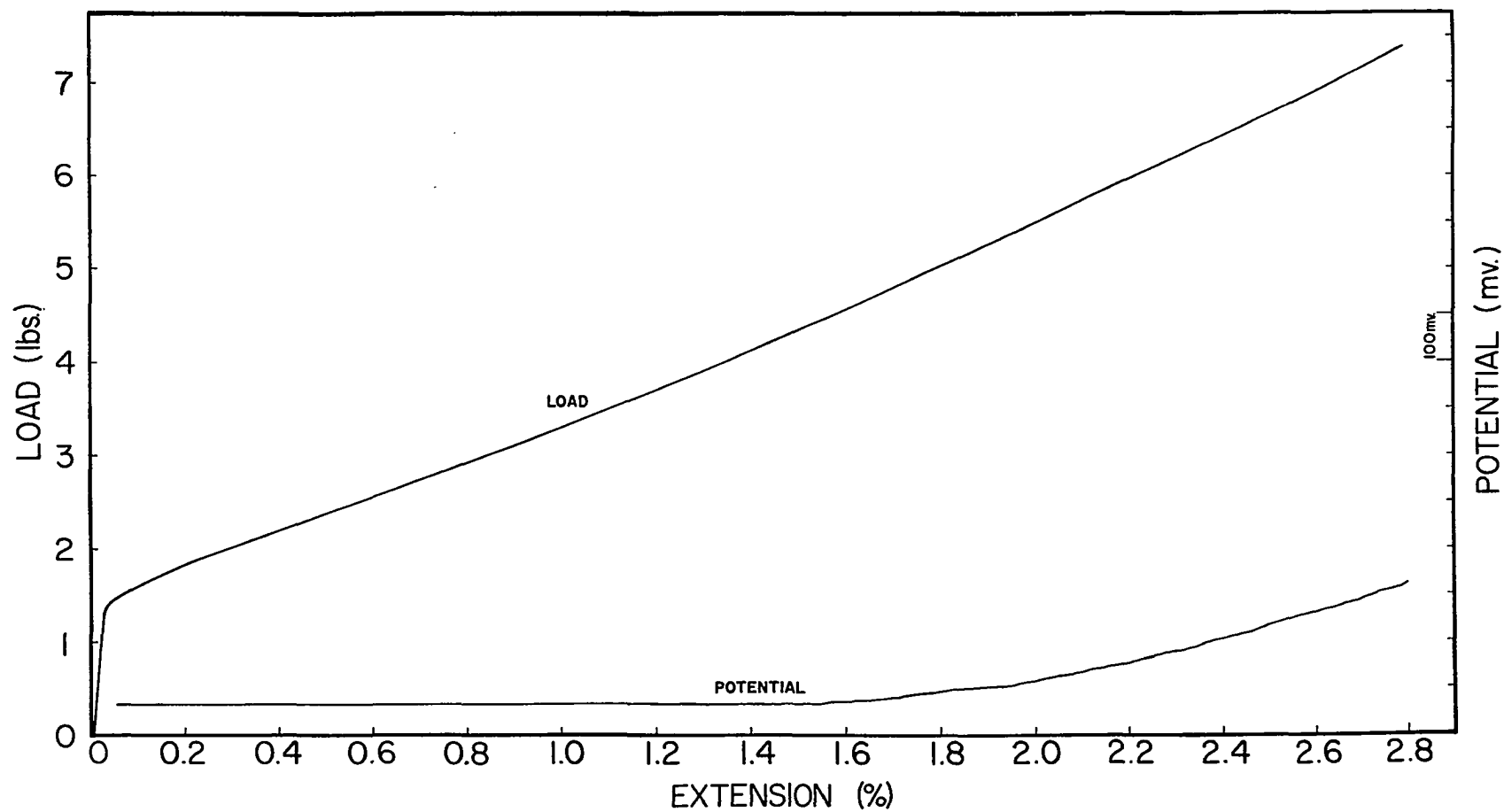


FIG. 25- Load-potential-extension curves for specimen R-7-5, coated with 300 Å thick anodic film.

cracking and fracture at the slip steps) of thin coatings, it is not possible to determine from the potential-elongation plot the exact strain at which transverse cracking begins. However, metallographic examination, immediately after film fracture was detected by the potential method, showed evidence of short transverse cracks as well as fracture at slip steps as discussed previously. Therefore, one can assume that transverse cracking took place concurrent with fracture at slip steps or shortly thereafter. The continuous rise in potential was due to continuous fracture at slip steps, and as was shown in Figure 12, a steady increase in the density of transverse cracks. Then it appears that the surface damage due to the transverse cracking of the anodic films was not only more severe for thick coatings (as was discussed in Part II) but also began at a much earlier stage of deformation of the substrate.

The lack of a reliable dislocation etch for aluminum precluded studies of the dislocation distribution and their depth of penetration underneath the cracks. Considering the etch pit results obtained from copper single crystals (14), one can deduce that elastic relaxation introduced a large number of dislocations at the surface in the vicinity of the cracks in the film. As the deformation continued, more and more of this surface damage occurred until crack saturation was reached. At this point, the preferential deformation became so strong as to influence the overall load-extension curve of the specimen as shown by the load drops in Figure 24.

The introduction of bands of high dislocation density on the surface of the aluminum single crystals can affect the Θ_1 through two related processes: (1) The intersection of these bands with the slip planes impedes the motion of glide dislocations and the activities of dislocation sources on these planes. (2) the localized stresses due to the preferential deformation could activate a large number of sources on the secondary slip system. Thus, while the bulk of the crystal is undergoing deformation in stage I, the surface would have deformation characteristic of stage II. These two processes may be partially responsible for the large increase in Θ_1 due to very thick (3000 Å) anodic coatings, reported in Table 5. However, this surface damage can not be

responsible for the changes in the parameters of stage I observed with the thinner anodic coatings. The relation between the fracture strain of the thin anodic coatings and the extent of easy glide in the aluminum (Figures 3 and 25) would limit the effect of "surface damage", on the mechanical properties of the substrate during the stage I deformation. Also the mode of fracture of the thin anodic coatings was such that extensive transverse cracking (which induced surface damage) required considerable substrate deformation (see Figure 12), corresponding to deformation of the aluminum single crystal well into stage II.

Summary:

The results presented in this section indicate that duration of easy glide (a_2) during stage I deformation was affected mainly by the state of residual stress induced on the surface of the crystals by the anodic coatings. Both thin and thick coatings changed the duration of easy glide according to the nature of residual stresses produced in the coatings. Coatings formed at high formation rates (2 ma/cm^2) and believed to have tensile residual stresses decreased the duration of easy glide. Coatings formed at low formation rate (0.2 ma/cm^2), and are believed to have had compressive residual stresses, reduced the duration of easy glide. It was proposed that the magnitudes of the residual stresses in the coatings were high enough to produce a stressed layer on the surface of single crystal specimens upon the completion of the formation process. In turn this surface layer can influence the length of easy glide by activation of the surface sources (34) and the flow stress gradient concept (43).

The thickness dependence of the Δa_2 was attributed to the changes in the magnitude of residual stresses as the coating thickness was increased (25,27).

The slope of stage I (Θ_1) was affected mainly by the ability of the coatings to block emergence of dislocations. Thus, $\Delta \Theta_1$ increased as the coating thickness was increased.

The relation between the fracture strain of the anodic coatings and the duration of easy

glide in aluminum limited the contribution of the "surface damage" to the changes in the stage I parameters.

Based on the information presented in this report, it appears that the duration and the rate of work hardening in stage I of the coated aluminum single crystals were affected by different parameters. The extent of stage I was mainly affected by the state of the residual stress, associated with the rate of formation of the anodic coatings. The slope of stage I was influenced by the ability of the coatings to inhibit the egress of dislocations.

REFERENCES

1. I.R. Kramer and L.J. Demer; Prog. Mat. Science, 9, 131, (1961).
2. A.R.C. Westwood: Environmental Sensitive Mechanical Behavior; 1, Gordon and Breach, New York, (1966).
3. R. Roscoe, Nature; London, 133, 912, (1934).
4. S. Harper and A.H. Cottrell, Proc. Phys. Soc., B63, 331, (1950).
5. J. Takamura, Mem. Fac. Engng., Kyoto Univ., 18, (3), 225, (1956).
6. E.N. daC. Andrade and C. Henderson, Phil. Trans. Roy. Soc., A244, 177, (1951).
7. C.S. Barrett; Acta Metallurgica, 1, 2, (1953).
8. C.S. Barrett, P.M. Aziz and I. Markson, Trans., AIME, 197, 1655, (1953).
9. D.B. Holt, Acta Metallurgica, 10, 1021, (1962).
10. T.H. Alden and W.A. Backofen, Acta Metallurgica, 10, 352, (1961).
11. B.I. Edelson and W.D. Robertson, Acta Metallurgica, 2, 503, (1954).
12. W.A. Jamin and C.C. Law, Acta Metallurgica, 15, 143, (1967).
13. J.C. Grosskreutz, Surface Science, 8, 173, (1967).
14. R.M. Johnson and R.J. Block, Acta Metallurgica, 16, 831, (1968).
15. A.K. Head; Phil Mag., 44, 92, (1953).
16. A.H. Cottrell; Dislocation and Plastic Flow in Crystals, Clarendon Press, Oxford, (1953).
17. J.C. Fisher; Trans. Met. Soc., A.I.M.E., 194, 531, (1952).
18. J.J. Gilman; Phil. Mag., 6, 159, (1961).
19. M.A. Adams; Acta Metallurgica, 6, 327, (1958).
20. M.S. Hunter and P. Fowle, J. Electrochem. Soc., 101, 481, (1954).
21. N.J. Cochrane and R.J. Block, J. Electrochem. Soc., 117, 225, (1970).
22. R.J. Block, J. Electrochem. Soc., 117, 788, (1970).

23. C. Edeleanu and T.J. Law, *Phil. Mag.*, 7, 573, (1962).
24. D.H. Bradhurst and J.S. Llewelyn Leach, *Trans. British Ceram. Soc.*, 62, 793, (1963).
25. D.H. Bradhurst and J.S. Llewelyn Leach, *J. Electrochem. Soc.*, 113, 1245, (1966).
26. A. Brenner and S.J. Senderoff, *J. Res. Nat. Bur. Stds.*, 42, 89, (1949).
27. D.A. Vermilyea, *J. Electrochem. Soc.*, 110, 345, (1963).
28. J.A. Davis, J. Domiji, J.P. Pringle, and F. Brown, *J. Electrochem. Soc.*, 112, 675, (1965).
29. D.R. Brames and T. Evans; *Phil. Mag.*, (viii) (33) 3, 971, (1958).
30. T. Evans and D.R. Schwarzenberger; *Phil. Mag.*, 4, 899, (1959).
31. J.C. Grosskreutz and M.B. McNeil, *J. Electrochem. Soc.*, 116, 9, 1233, (1969).
32. R.J. Block and M. Metzger, *Phil. Mag.*, 19, 599, (1969).
33. J.J. Gilman and T.A. Read, *Trans. of Metals Soc., AIME*, 194, 875, (1952).
34. F.J. Worzala and W.H. Robinson, "Environmental Sensitive Mechanical Behavior", Gordon and Breach, New York, (1966).
35. K. Sumino, *J. Phys. Soc., Japan*, 17, 454, (1962).
36. S. Mendelson, *J. Appl. Phys.*, 33, 7, 2188, (1962).
37. T. Suzuki, "Dislocations and Mechanical Properties of Crystals", 215, John Wiley & Sons Inc., New York, (1957).
38. J.J. Gilman and W.G. Johnson, "Dislocations and Mechanical Properties of Crystals", 215, John Wiley & Sons inc., New York, (1957).
39. M.A. Adams, *Acta Metallurgica*, 6, 327, (1958).
40. P.B. Hirsch, "Relation Between Structure and Mechanical Properties of Metals", Her Majesty's Stationary Office, London, 39, (1963).
41. R.M. Latanision and R.W. Staehle, *Acta Metallurgica*, 17, 307, (1969).
42. S.N. Buckley and K.M. Entwistle, *Acta Metallurgica*, 4, 352, (1956).
43. J.T. Fourie, *Proc. Inter., Conference Deformation of Crystalline Solids, Ottawa*, 777, (1966); *Phil. Mag.*, 17, 735, (1968).

44. J.J. Hauser and B. Chalmers, *Acta Metallurgica*, 9, 802, (1961).
45. A.P. Boresi, "Elasticity In Engineering Mechanics", 101, Prentice Hall Inc., Englewood Cliffs, New Jersey, (1965).
46. A.J. Durelli, E.A. Phillips, and C.H. Tsao, "Introduction to the Theoretical and Experimental Analysis of Stress and Strain", 337, McGraw-Hill, New York, (1958).

APPENDIX A

The object of this section is to develop relations between the shear strain in the bulk of the single crystal specimen and the strain components on the surface of the crystal, which affect the deformation of the anodic films.

If a single crystal specimen, shown in Figure A1, shears homogeneously by an amount γ on its primary slip system, the strain at the boundary between the specimen surface and the coating can be described in terms of six strain components: $e_{xx}, e_{yy}, e_{zz}, e_{xz}, e_{yz}, e_{xy}$. For small shear strains, the relation between γ and the strain components of interest to film fracture can be obtained from the work of Hauser and Chalmers (44):

$$\begin{aligned} e_{yy} &= l\gamma & e_{xz} &= p\gamma \\ e_{zz} &= m\gamma & e_{yz} &= q\gamma \\ e_{xx} &= n\gamma \end{aligned}$$

where:

$$\begin{aligned} l &= (\bar{y} \cdot \bar{e}) (\bar{y} \cdot \bar{g}) & p &= 1/2 [(\bar{z} \cdot \bar{e}) (\bar{z} \cdot \bar{g}) + (\bar{x} \cdot \bar{e}) (\bar{x} \cdot \bar{g})] \\ m &= (\bar{z} \cdot \bar{e}) (\bar{z} \cdot \bar{g}) & q &= 1/2 [(\bar{y} \cdot \bar{e}) (\bar{y} \cdot \bar{g}) + (\bar{z} \cdot \bar{e}) (\bar{z} \cdot \bar{g})] \\ n &= (\bar{x} \cdot \bar{e}) (\bar{x} \cdot \bar{g}) \end{aligned}$$

\bar{y} = unit vector along the Y axis.

\bar{z} = unit vector along the Z axis (Tensile Axis).

\bar{x} = unit vector along the X axis.

\bar{e} = unit vector normal to the slip plane.

\bar{g} = unit vector parallel to the slip direction.

Since the coating is thin, we can also assume that stresses perpendicular to the surface are negligible throughout the coating thickness. Then, for all practical purposes, the

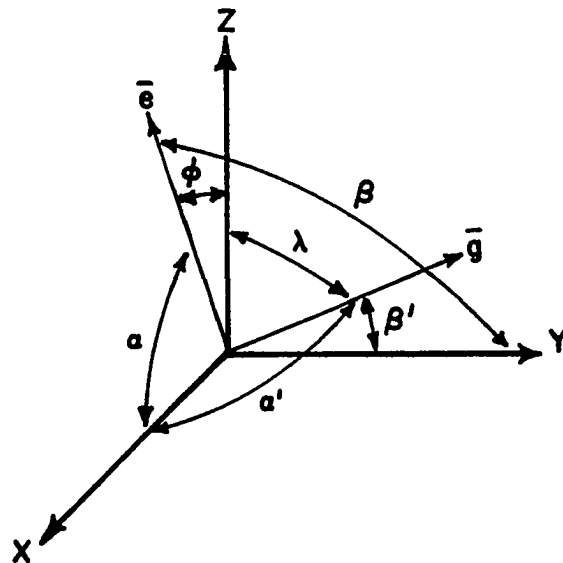
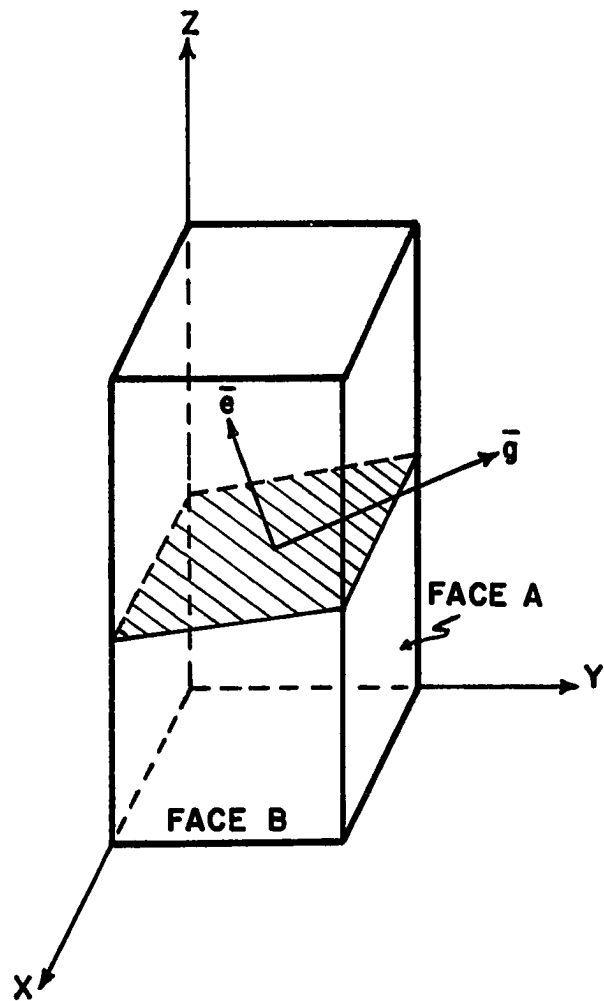


FIG. AI- Geometric conventions used in the calculation of the strain components and the crack angles.

coating is considered to be under the action of plane stresses. The adherence between the coating and the surface is also assumed to be perfect so the strains in the coating are identical to the strains on the surface of the specimen. The strain components that cause the transverse cracks on each face of the square crystal can now be written as:

Face A

$$\begin{aligned} e_{zz} &= m\gamma = \gamma \cos \varnothing \cos \lambda \\ e_{xx} &= n\gamma = \gamma \cos \alpha \cos \alpha' \\ e_{xz} &= p\gamma = \frac{\gamma}{2} (\cos \varnothing \cos \lambda + \cos \alpha \cos \alpha') \end{aligned}$$

Face B

$$\begin{aligned} e_{zz} &= m\gamma = \gamma \cos \varnothing \cos \lambda \\ e_{yy} &= l\gamma = \gamma \cos \beta \cos \beta' \\ e_{zy} &= \gamma = \frac{\gamma}{2} (\cos \varnothing \cos \lambda + \cos \beta \cos \beta') \end{aligned}$$

where $\alpha, \alpha', \beta, \beta' \dots$ etc. are the angles shown in Figure A1. The values for these angles were obtained from the stereographic projections of the surfaces, by the Laue back reflection technique, and are reported in the Table A1. The values of the strain components are reported in Table A11. We shall also assume that the brittle oxide coating cracks according to the maximum-tensile-strain law. Then, the cracks will appear perpendicular to the direction of the larger principal strain. Therefore, one can find the crack angle by calculating the deviation of the larger principal strain direction relative to the tensile axis (Z direction). This angle (Θ) is obtained from the relation (45):

$$\begin{aligned} \tan 2\Theta_A &= 2 e_{zx} / (e_{zz} - e_{xx}) = \frac{\cos \varnothing \cos \lambda + \cos \alpha \cos \alpha'}{\cos \varnothing \cos \lambda - \cos \alpha \cos \alpha'} \\ \tan 2\Theta_B &= 2 e_{yz} / (e_{zz} - e_{yy}) = \frac{\cos \varnothing \cos \lambda + \cos \beta \cos \beta'}{\cos \varnothing \cos \lambda - \cos \beta \cos \beta'} \end{aligned}$$

Values of Θ (the crack angle) shown in the Table 2 were obtained from the above relations.

TABLE AI

Values of different angles used in the calculation of
the principal strains and the crack angles (degree)

Specimen Designation	ϕ	λ	α	α'	β	β'	Θ_A	Θ_B
S-4A	53.5	37.3	70	111	42	119	15.0	4.1
S-4B	42	47	44.5	137	86	97	1.5	17.4

TABLE AII

Values of the strain components used in the calculation of the
principal strains. All strains are in terms of fraction of shear strain (γ)

Specimen Designation	e_{zz}	Face A		Face B	
		e_{xx}	e_{xz}	e_{yy}	e_{yz}
S-4A	0.476	-0.122	0.177	-0.354	0.061
S-4B	0.470	-0.522	0.026	-0.085	0.193

PRINCIPAL STRESS FUNCTIONS:

The stress components on the specimen faces can be obtained from the strains by using the following relations:

$$\sigma_{ii} = \frac{(1-\nu) E \epsilon_{ii}}{(1+\nu)(1-2\nu)} + \frac{\nu E \epsilon_{jj}}{(1+\nu)(1-2\nu)}$$

$$\sigma_{ij} = \frac{E}{2(1+\nu)} \gamma_{ij}$$

Thus the stress components on the face A of each specimen are (see Figure A1):

$$\begin{aligned} \sigma_{zz} &= \frac{E_s \gamma}{1+\nu_s} \left[m + \frac{\nu_s}{1-2\nu_s} (m+n) \right] \\ \sigma_{xx} &= \frac{E_s \gamma}{1+\nu_s} \left[n + \frac{\nu_s}{1-2\nu_s} (m+n) \right] \\ \sigma_{xz} &= \frac{E_s \gamma}{2(1+\nu_s)} p = \frac{E_s \gamma}{4(1+\nu_s)} (m+n) \end{aligned}$$

where E_s and ν_s are the Young's modulus and Poisson's ratio of the substrate aluminum.

The principal stresses on this face can be calculated from:

$$\sigma_1^s, \sigma_2^s = \frac{\sigma_{zz} + \sigma_{xx}}{2} \pm \left[\left(\frac{\sigma_{zz} - \sigma_{xx}}{2} \right)^2 + \sigma_{xz}^2 \right]^{1/2}$$

where σ_1^s and σ_2^s are the principal stresses in the specimen. The principal stress in the coating (σ_1^c) shown in the Table 2, were obtained from specimen principal stresses by using the following relation (46):

$$\sigma_1^c = \frac{E_c}{E_s(1-\nu_c^2)} \left[(1-\nu_c\nu_s) \sigma_1^s + (\nu_c - \nu_s) \sigma_2^s \right]$$

where E_c and ν_c are the Young's modulus and the Poisson's ratio of the coating. For the stress functions shown in Table 2, it was assumed that $\nu_s = 0.32$ and $\nu_c = 0.2$.

APPENDIX B

The following computer program was used to obtain shear-stress vs. shear-strain plots from the load vs. extension data:

```

      DIMENSION          P(300),XXL(300)
      CONV=57.29577951
      READ(2,1) CXL,A1,A2,CSA,N
1  FORMAT(4F10.6,I5)
      WRITE(3,2) A1,A2
2  FORMAT(1X,7HLAMDA= ,F7.3,5X,5HPHI= ,F7.3)
      WRITE(3,3)
3  FORMAT('  INSTANTANEOUS          SCHMIDT          RESOLVED
1')
      WRITE(3,4)
4  FORMAT('  GAGE LENGTH          FACTOR          SHEAR STRESS
2N ',//)
      CSAM=CSA*645.1613
      A=A1/CONV
      B=A2/CONV
      C=SIN(A)
      SX=225.
      SY=.04
      J=1
      CALL EPLLOT(2,0.,0.)
      CALL SCALE(SX,TY,0.,0.)
      CALL EGRID(1,0.,0.,50.,12)
      CALL EGRID(0,0.,0.,.01,16)
      CALL EPLLOT(0,0.,0.)
      DO 10 I=1,N
      READ (2,5)  XXL(I),P(I)
      XL=XXL(I)+CXL
5  FORMAT(2F10.5)
      Q=P(I)*453.5924277
      D=CXL*C/XL
      E=ATAN(D/SQRT(1.0-D**2))
      SM=COS(B)*COS(E)
      S=(SQRT((XL/CXL)**2-C**2)-COS(A))/COS(B)
      T=Q*SM/CSAM
      WRITE(3,6) XL ,SM,T,S
6  FORMAT(F15.6,3F15.7)
      CALL EPLLOT(-2,S,T)
      CALL POINT(J)
      CALL EPLLOT(1,S,T)
10 CONTINUE
      CALL EXIT
      END

```

APPENDIX C

The following program was used in conjunction with the GE 430 Computer System to determine the slopes of stages I and II from the shear strain - shear stress data:

```
140 CALL OPENF (1, "THETA")
150 READ (1. ) X1, Y1
200 X=X1
250 Y=Y1
300 4 READ (1. ) X1, Y1
350 V=X-X1
400 W=Y-Y1
450 Z=V/W
500 PRINT, X1,Y1,Z
550 X=X1
600 Y=Y1
750 GO TO 4
800 END
```